NGR-22-009-123

Earth Models Consistent with Geophysical Data

Frank Press

Department of Earth and Planetary Sciences

Massachusetts Institute of Technology

Cambridge, Mass. U.S.A.

ABSTRACT

A suite of the most recently available geophysical data are inverted by an improved Monte Carlo procedure. The data are derived from surface waves for oceanic paths, eigenvibrations of the earth, elastic wave travel time and dt/dΔ data, mass and moment of inertia of the earth. A low velocity zone is required for the suboceanic mantle as is a high density lithosphere. The high density is related to eclogite fractionation from the underlying, partially molten asthenosphere in a process involving the creation and spreading of the lithosphere. If the asthenosphere is pyrolite or peridotite then an increase of mean atomic weight across the transition zone seems required. Fairborn's new dt/dΔ data for the lower mantle seem to show a higher shear velocity gradient than previously supposed. If correct, a compensatory lower density gradient is required. This may indicate a depletion of iron with depth in the lower mantle. The density at the top of the core is surprisingly well constrained to the range 9.9-10.2 gm/cc, a value appropriate for a mixture of iron and about 15 wt % silicon.

I. Introduction

A major goal of geophysics is to uniquely specify the distribution of two elastic velocities and density with depth in the earth and to relate these distributions to variations in composition, phase, and temperature in the interior. Impediments which block these achievements are many. It has not been proved in the mathematical sense that a unique solution can be obtained, although BACKUS and GILBERT (1968) have shown that under certain circumstances stable weighted averages (over depth) can be calculated. Furthermore, the data set available for recovering earth structure is incomplete and imprecise. Finally the equations of state available for interpreting elasticity and density distributions in terms of composition, state, etc.are tentative ones based on uncertain theories and assumptions and limited laboratory data.

Despite these difficulties it may be possible even with the presently available data to make some meaningful statements about the interior. In this paper we explore this possibility using the most recent and best available data in a Monte Carlo inversion procedure. Our results and conclusions supersede those presented in earlier papers (PRESS, 1968 a & b) because we are able to fit models to new, more extensive and accurate data with greater speed and better precision.

II. Method

The Monte Carlo method uses random selection to generate large numbers of models in a computer, subjecting each model to a test against geophysical data. Only those models are retained whose properties fit the data within a prescribed tolerance. The procedure offers the advantage that successful models are found without bias, preconceived ideas or uncertain assumptions of equations of state or composition. If the program is efficient so that a very large number of models are examined, the retained models can be considered as representative of the family of successful models which fit the data. When the successful models fall in a narrow band, geophysically meaningful conclusions can often be reached despite our inability to specify a single unique model. Under certain conditions (BACKUS and GILBERT 1968) a single successful model can provide unique, local averages of density or velocity.

We have modified the Monte Carlo procedure reported last year (PRESS, 1968 a) speeding up the process by 1-2 orders of magnitude. This improved efficiency enabled us to find a larger number of successful models fitting a more extensive suite of data with better precision. The flow diagram of the currently used system (fig. 1) is printed with each run of the program and provides diagnostics so that controlling constants can be set for maximum efficiency. The figure shows the diagnostics following a run of 3347 seconds on an IBM 360-65 computer which yielded 11 successful models at a cost of about $10 per successful model. SLMD is the random selection procedure for compressional velocity (alpha), shear velocity (beta) and density (rho). TTT is a test of the model against observed travel times using BULLEN'S (1961) method in which the earth is treated as a multi-layered sphere, the velocity varying according to a power law within each layer. VRPR uses a table of variational parameters (WIGGINS 1968) stored permanently in a data cell of the computer to test the perturbation of the eigenperiods due to velocity, density or core radius perturbations. This test is made after the selection of density and velocity models, the latter in order to eliminate early in the process those models which cannot be brought into agreement with eigenperiod data by density perturbations. MASMOM tests each density model against mass and moment of inertia of the earth. The flow diagram shows branching according as the several tests are passed or failed. Each box shows the number of times the corresponding step was repeated, the average time and total time for each step and the percentage of model passing. Thus the time distribution over the various components of the program is available for adjustment of input constants for maximum efficiency and insight is provided as to how the various geophysical constraints figure in the elimination of models. A key requirement of the Monte Carlo method is that the selection procedure produce an unbiased, representative suite of models for examination. Figures 2, 3, and 4 show a run in which 25 models were generated, bypassing tests against geophysical data. It is seen that the velocity and density space between the permissible bounds is nearly uniformly filled. Since millions of earth models were generated and examined in this study it would be surprising if continued operation of the program would produce a successful model significantly different from those presented later in this paper. Some additional features of the program and procedures used are as follows:

1. The earth is assumed to be spherically symmetrical and isotropic, with an oceanic crust-upper mantle structure. The radius of the core is selected randomly for each model in the range 3473 $\pm$ 25 km.
2. Although α, β, ρ could be varied at 88 points in the earth, we chose the time saving device of randomly varying 19 points, (see fig. 5, section D for their location) obtaining the remaining values by linear interpolations.
3. The fluid core was assumed to be adiabatic. The density selection procedure for the mantle below 1000 km eliminated models with extreme density gradients. The gradients in α, β, ρ were restricted to a maximum number of reversals in sign (typically 2 or 4) to restrict the complexity of models.
4. The rigidity for the inner core only affects the mode ${}_0S_2$. Although zero rigidity was assumed in this paper, the

systematic, negative residuals for ${}_0S_2$ found in our models will be used to infer a rigidity for the inner core.

5. Several exact calculations of eigenperiods were made to check the accuracy of the variational parameter method. The differences were small and well within the uncertainty of the data.

III. The Data

Successful models were required to fit the following data:

1. Earth mass, M=5.976 x 10^{27} grams; dimensionless moment of inertia I/Ma^2= .3308

2. Compressional velocity distribution in the mantle fixed very close to the models determined by JOHNSON (1969) and FAIRBORN (1969), based on dt/dΔ analyses of array data. P and PcP travel times fit the latest data (HERRIN et al. 1968) to $\pm$ 1 sec. The compressional velocity distribution in the core was fixed to the recent model of HUSEBYE and TOKSÖZ (1969).

3. Shear velocities below 800 km were restricted to lie within the narrow bounds reported by FAIRBORN (1969) who used Monte Carlo methods to interpret travel time and dt/dΔ data obtained from the Large Aperture Seismic Array (LASA). Wider bounds were used above 800 km. Travel times of S and ScS were required to fit FAIRBORN'S data to within $\pm$ 5 sec at 10 distances between 25° and 100° and a single failure was sufficient to reject a model. These travel time data primarily constrain the mantle below 800 k

4 Eigenperiods tested were ${}_0S_0$, ${}_0S_2$ through ${}_0S_{22}$, ${}_1S_2$, ${}_1S_3$, ${}_1S_5$, ${}_1S_6$, ${}_1S_8$, ${}_1S_{12}$, ${}_2S_4$, ${}_2S_6$, ${}_2S_{10}$; toroidal oscillations tested were ${}_0T_3$-${}_0T_{21}$, ${}_0T_2$ not being used because of its uncertain value; models were also required to fit surface wave phase velocities for predominantly oceanic paths as follows: Rayleigh waves in the period range 125-325 seconds (BEN-MENAHEM, 1965); Love waves in the period range 80-340 seconds (TOKSOZ and ANDERSON, 1966). We used the eigenperiod data as reviewed and summarized by DERR (1969)

except as follows: ${}_{o}S_{2}$- 3229.0 seconds, ${}_{o}S_{11}$- 537.5 seconds. The uncertainty in the eigenperiod and dispersion data was taken to be $\pm$ 0.4% due to asphericity, rotational splitting and experimental errors (DAHLEN 1968). An error analysis of the oceanic surface wave data indicates than an accuracy better than 1% was achieved. Comparison with phase velocities for other oceanic paths verified this for Love and Rayleigh waves. The fit of ${}_{o}S_{o}$ was required to be within $\pm$ 0.1%. Actually the final models fit most of the data to about half these tolerances. Figure 5 shows the computed eigenperiods and the residuals for a typical model.

IV. Results

The results reported here supersede our earlier conclusions (PRESS 1968) because of the new and more extensive data set inverted in this paper. The effects of lateral variation were reduced by deriving higher mode data from oceanic surface wave phase velocities. Moreover the new procedure enabled us to find a much larger number of successful models and therefore a more representative selection from the set of successful models.

The shear velocity and density distribution are plotted in figs. 6,7, and 8 and are also tabulated (together with the fixed compressional velocity distribution) in figs. 9-13.

V. The Upper Mantle Under Oceans

Without exception every successful model contains a low velocity zone for shear waves which centers at depths between 150 and 250 km. If the lid of this zone is characterized by $\beta >$ 4.5 km/sec, then its thickness is 50-100 km. We failed to find a single model without a low velocity zone despite a special search in which 162,000 monotonic shear velocity models were examined. A low velocity zone seems required by our data since essentially every possible model without it was examined and eliminated. Nevertheless, HADDON and BULLEN (1969) reported a successful monotonic model, probably because: (1) they only use modes through n=44, whereas our data go to n=105; (2) our Love wave phase velocities trend towards lower values than the HB data (see fig. 14).

The several mechanisms which might account for the low velocity partial (grain boundary) melting for the following reasons: (1) shear velocity and Q are sensitive to the presence of small amounts of melt along grain boundaries; (2) data presented at this conference by several investigators show that the temperature at which melting begins in the wet state for candidate upper mantle mineral assemblages is sufficiently low to be reached by the geotherm for most thermal models of the earth; (3) the partial melting product of candidate mineral assemblages can account for basaltic vulcanism; (4) a partially molten, low strength zone would serve to mechanically decouple the lithosphere from the underlying mantle as is required by some proposed mechanisms for the spreading sea floor.

The density values shown in figs. 7 and 15 fill the entire permissible range at the M-discontinuity indicating a lack of constraint by the geophysical data. However, the initial density gradients are all positive and in the vicinity of 100 km all the values fall in the narrow band 3.5-3.6 gm/cm^3 in the upper part of the permissible range. As a check on this result a special search was made without success to find models with densities below 3.4 gm/cm^3 in this depth range. For additional confirmation of this result we applied the BACKUS and GILBERT (1968) δ-ness criterion using weighting functions computed for our data by WIGGINS (1969). According to Backus and Gilbert, if the weighting functions are concentrated over narrow depth intervals, a stable local average can be obtained from a single model. Using this procedure every one of the models yielded an average density in the range 3.5-3.6 g/cm^3 for the depth interval 75-125 km. Presumably the average density near 100 km is uniquely determined in the sense that any model computed from our data set should give the same value.

Unfortunately the density resolution deteriorates below 100 km as can be seen by the wider band of Monte Carlo solutions. At

300 km the resolving length inferred from the δ-ness criterion is 200 km. One might argue on physical grounds that the lower density solutions should be favored below 150 km because of the low shear velocities. This implies a density reversal from the lithosphere to the asthenosphere (3.5-3.6 gm/cm^3 at 100 km to 3.3-3.5 gm/cm^3 at 300 km).

More complex models were found involving two low velocity or two low density zones in the upper mantle. However, these models yield the same indication of high density near 100 km.

The indicated density for the lithosphere near 100 km is so high as to narrow the range of its possible composition to an eclogitic facies. This follows if the selection is made from the current petrologic hypotheses for the constitution of the upper mantle. In fig. 15 densities computed by CLARK and RINGWOOD (1964) for a mantle composed of pyrolite (peridotite or dunite would give about the same values) and eclogite. Only the eclogite model is consistent with our results between 80 and 150 km. Either model is acceptable above this region and the pyrolite model is weakly favored near 300 km. A more extended discussion of these results can be found in another paper (PRESS 1969) where a hypothesis is proposed in which eclogite fractionation from the underlying, partially molten asthenosphere is involved in the creation and spreading of the sub-oceanic, rigid, lithospheric plate. BIRCH (1969) also interpreted these results to imply an eclogitic composition.

VI. The Transition Zone

Seismic array data have been used recently to establish rapid velocity changes near 400 and 700 km (see for example JOHNSON, 1967). These results have been incorporated in our models by fixing the compressional velocity and narrowing the range of permissible shear velocities at these depths to conform to the rapid increases, as seen in fig. 6. Although no such restrictions were placed on the density values the rapid increase in density across the transition zone is evident on all models in fig. 7. This increase is due to compression, and to phase changes and possibly to composition changes. Phase transitions are/also inferred from the laboratory verification of the olivine-spinel phase change at pressures corresponding to depths near 400 km and by the theoretical and experimental indications for a post-spinel phase transformation. (See for example, D.L. ANDERSON (1967) or H. FUJISAWA (1968)).

The occurrence of composition changes in the transition zone are more difficult to establish. BIRCH (1961) used the velocity change $\Delta\alpha$, and the density change $\Delta\rho$ to separately estimate the effects of phase and composition change. Using $\Delta\alpha$ and $\Delta\rho$ values for each model between 333 and 871 km, allowing .36 gm/cc for compression and using Birch's values for $(\partial\alpha/\partial\rho)_m$, $(\partial\rho/\partial m)_{T,P}$, $(\partial\alpha/\partial m)_\rho$, the change in mean atomic weight Δm was computed across the transition zone for each model. Those models with reduced densities in the asthenosphere ($\rho < 3.4$ gm/cc) showed an increase of 1-2 units in m. Thus for an asthenosphere with $m \sim 21$, and Fe/Fe + Mg $\sim$ 0.1, as would be the case for peridotite or pyrolote, the Fe/Fe + Mg ratio would increase to 0.2 or 0.3 across the transition zone. On the other hand, no increase in m was found for those models with a high density asthenosphere ($\rho > 3.5$ gm/cc). If the entire upper mantle is closer to eclogite in its iron content no increase in the Fe/Fe + Mg ratio seems to be required across the transition zone. In a recent paper D.L. ANDERSON (1968) proposed that $\Delta m \sim 1.5$ and BIRCH (1961) gave $\Delta m \sim 1.0$ for one model.

VII. The Lower Mantle

Our results for the lower mantle rest heavily on Fairborn's independent determinations of a band of shear velocity distributions consistent with $dt/d\Delta$ and travel time data obtained at LASA. The range of shear velocities permitted by Fairborn's results is quite narrow, as can be seem in fig. 6. This enables us to use eigenperiod data to constrain the density in the lower mantle to a greater degree than was possible before. Fairborn's shear velocity envelope shows a higher gradient than has usually been assumed (e.g. when compared to the Gutenberg model) and this requires a compensatory reduction in the density gradient in order to fit the spheroidal eigenperiod data. The results are shown in figs. 6 and 7. The density is constrained surprisingly well, to within about 0.2 gm/cc for most of the lower mantle. The density gradient is less than the adiabatic gradient as can be seen by comparison with the lower bound which approximates an adiabatic gradient. Figure 16 shows our band of solutions plotted against D.L. ANDERSON'S (1968) theoretical calculations for density of the solid solution series forsterite-fayalite and his summary of shock wave data. The band of density solutions is discordant with respect to profiles of constant composition, suggesting a change of mean atomic weight from 22-23 at the top of the lower mantle to 20-22 at the bottom of the mantle. This implies a depletion of iron with depth with the Fe/Fe + Mg ratio going from 0.2-0.3 to 0.1-0.2. Although superadiabatic temperature gradients might also account for the smaller density gradient, the augmented shear velocity gradient argues against this.

This can also be seen in figure 17 where the bulk sound velocity and density values for each model are plotted. The figure also shows the shock wave values for Twin Sisters dunite ($m=20.9$) and hortonolite dunite ($m=25.1$), as reduced by AHRENS, ANDERSON and RINGWOOD (1969). Although the data are scanty, a reduction in mean atomic weight from 22-23 at 871 km to 20-21 at 2898 km is indicated. The discordance with lines of constant composition seems too large to be accounted for by superadiabatic temperature gradients. WANG (1969) also suggested that these data might indicate decreasing m in the lower mantle. If subsequent studies do not establish Fairborn's shear velocity distribution as a world wide phenomenon, this conclusion will have to be changed.

VIII. The Mantle

The c-ρ graph illustrates the main features of the mantle discussed earlier. The olivine-spinel phase transformation is evidenced between 371 km and 421 km by models with increasing c and ρ. Between 421 km and 621 km models with large increases in ρ and with little change in c could be interpreted as the result of compression and increasing iron content, the two effects having the same sign for ρ and opposite signs for c. The increase in c and ρ between 621 km and 721 km implies a phase change as the major feature. Decomposition of the ferro-magnesium-alumininum silicate to close packed simple oxides, or transformations to structures such as ilmenite or perovskite have been suggested for this region (BIRCH 1952, D.L. ANDERSON 1967, RINGWOOD 1969).

The distributions for ϕ and k/μ in the mantle are given in figs. 18 and 19.

XI. The Core

Results for the core are shown in figs. 8 and 20. The assumption of adiabaticity in the fluid core and the constraints imposed by the data prescribe the densities to the surprisingly small range of .25 gm/cc. The δ-ness criterion also indicates high resolving power for density at the top of the core. Using the shock wave data of McQUEEN and MARSH (1966) and BALCHAN and COWAN (1966) we see that iron alloyed with a miscible, abundant element such as silicon (15 wt %) would account for the core densities. There is no control on the density in the inner core with the data used here. Changes in the core radius ranged from -3 km to + 10 km.

The requirement for finite rigidity of the inner core was evidenced in an interesting way. Our procedure neglects core rigidity and the only mode affected by this assumption, ${}_0S_2$ showed negative residuals for every model. Using ALSOP'S (1963) correction for rigidity resulted in a reduction of the residuals, for ${}_0S_2$, the largest discrepancy being .15%. This agrees with D.L. ANDERSON'S conclusions concerning rigidity in the inner core (1969).

X. Discussion

The question of uniqueness arises in all discussions of internal earth structure. The Backus-Gilbert δ-ness criterion demonstrates how stable local averages can be computed for α, β and ρ using eigenperiod data. However with currently available data the resolving power is adequate at too few places in the earth. Also the procedure does not yet allow for travel time or $dt/d\Delta$ data which under certain circumstances have high resolving power, nor does it consider errors in data. The band of solutions provided by the Monte Carlo method, if sufficiently narrow and if derived without bias from a large and representative selection of models, can under certain circumstances lead to meaningful conclusions. Unfortunately one is never quite sure that continued search would not reveal models significantly different from those already found, vitiating the conclusions. The use of physical arguments, laboratory experiments, theoretical-empirical equations of state will eventually provide powerful constraints. However the poor state of knowledge of the behavior of materials at internal earth pressures and temperatures, though improving rapidly, is a severe, current limitation.

With regard to the present paper and the other studies cited, we believe the following results are firm if the assumptions and data are correct:

1. The low velocity zone for shear waves in the sub-oceanic upper mantle. The parameterization included sufficiently few elements so that all possible models without a low velocity zone

could be tested and eliminated.

2. The high density for the lithosphere near 100 km. The δ-ness criterion has high resolving power for density at this depth and the narrow spread of Monte Carlo solutions indicate that errors in surface wave data of about ~~10%~~ 1% do not weaken the constraint. As mentioned earlier, we believe this accuracy was achieved.

3. The rapid velocity increase near 400 km and its association with the olivine-spinel transformation: directly obtainable from $dt/d\Delta$ data (with minor depth uncertainty); the phase transformation was experimentally verified in the laboratory and olivine is almost certainly a major constituent of the upper mantle.

4. The rapid velocity increase near 700 km: directly obtainable from $dt/d\Delta$ data (with some depth uncertainty).

5. The density at the top of the core is between 9.9 and 10.2 gm/cc. The δ-ness criterion shows high resolving power and the spread of Monte Carlo solutions is small.

XI. Acknowledgements

Joel Karnofsky was an invaluable research assistant in this project. R.A. Wiggins kindly made his δ-ness weighting functions available in advance of publication. D.L. Anderson, F. Birch, C. Wang, J. Fairborn, K.E. Bullen, J.Derr, M.N. Toksöz, made manuscripts available in advance of publication. A grant from the Australian National University made it possible for me to participate in this Symposium. The technique was developed as part of an inversion procedure for lunar data with support from the National Aeronautics and Space Administration under grant NGR 22-009-123. The application to the earth was supported by the Advanced Projects Research Agency and monitored by the Air Force Office of Scientific Research under contract AF 49(638)-1632.

Figures

Figure 1 - Flow diagram of Monte Carlo program during a run in which 531, 881 density models and 5025 shear velocity models were tested and yielded 11 successful models.

Figure 2 - Twenty-five shear velocity models of the mantle not subjected to geophysical constraints to test distribution of randomly generated models.

Figure 3 - Unconstrained mantle densities (see Figure 2 caption).

Figure 4 - Unconstrained core densities (see Figure 2 caption).

Figure 5 - Results for a typical model. Section A line 1: mass and moment of inertia; lines 2-4: p, Δ, theoretical times, model times and residuals for S and ScS. Section B: model eigenperiods and residuals against observed eigenperiods. Section C: model printout. Section D: depths at which parameters were varied and corresponding $\mathfrak{m}$ values.

Figure 6 - Twenty-seven successful shear velocity models for the mantle. Ticks on upper and lower bounds show where parameter was randomly varied.

Figure 7 - Density in the mantle (see Figure 6 caption).

Figure 8 - Density in the core (see Figure 6 caption).

Figure 9 - Tabulated parameters of successful models. Change in core radius shown in lower right corner. Each model has fixed crustal layers for depth, alpha, beta and rho as follows: 0., 1.52, 0. 1.03; 3., 6.55, 3.73, 2.84; 10, 6.55, 3.73, 2.84.

Figure 10 - See Figure 9

Figure 11 - See Figure 9

Figure 12 - See Figure 9

Figure 13 - See Figure 9.

Figure 14 - Differences in Love wave phase velocity data used by Hadden and Bullen and by Press which accounts for latter's requirement of low velocity zone. Points show how models fit the data.

Figure 15 - Successful density models for the upper mantle plotted together with Clark and Ringwood models for pyrolite and eclogite.

Figure 16 - D. L. Anderson's theoretical models and his summary of experimental data plotted with our density solutions shown by the shaded band.

Figure 17 - Bulk sound velocity-density plot for successful models of the mantle together with static and shock wave data for dunite and forsterite-fayalite.

Figure 18 - Seismic parameter ϕ for the mantle obtained from successful models.

Figure 19 - Ratio K/μ for the mantle obtained from successful models.

Figure 20 - Band of core densities from successful models together with shock wave density data for Fe, Ni and Fe+ 19.8 wt.% Si.

REFERENCES

AHRENS, T.J., D.L. ANDERSON and A.E. RINGWOOD (1969), in press.

ALSOP, L.E. (1963), Bull. Seismol. Soc. Am., 53, 503.

ANDERSON, D.L. (1967), Science, 157, 1165.

ANDERSON, D.L. (1968), Earth and Planet. Sci. Let., 5, 89.

ANDERSON, D.L. (1969), this volume.

BACKUS, G., and F. GILBERT (1968), Geophys. J., 16, 169.

BALCHAN, A.S., and G.R. COWAN (1966), J. Geophys. Res., 71, 3577.

BEN-MENAHEM, A. (1965), J. Geophys. Res., 70, 4641.

BIRCH, F. (1952), J. Geophys. Res., 57, 227.

BIRCH, F. (1961), Geophys. J., 4, 295.

BIRCH, F. (1969), this volume.

BULLEN, K.E. (1961), Geophys. J., 4, 93.

CLARK, S.P., and A.E. RINGWOOD (1964), Rev. Geophys., 2, 35.

DAHLEN, F.A. (1968), Geophys. J., 16, 329.

DERR, J. (1969), in press, Bull. Seismol. Soc. Am.

FAIRBORN, J.W. (1969), in press, Bull. Seismol. Soc. Am.

FUJISAWA, H. (1968), J. Geophys. Res., 73, 3281.

HADDON, R.A.W. and K.E. BULLEN (1969), in press.

HERRIN, E., W. TUCKER, J. TAGGART, D.W. GORDON, and J.L. LOBDELL (1968), Bull. Seismol. Soc. Am., 58, 1273.

HUSEBYE, E.S. and M.N. TOKSOZ (1969), in press, J. Geophys. Res.

JOHNSON, L.R. (1967), J. Geophys. Res., 72, 6309.

JOHNSON, L.R. (1969), in press.

McQUEEN, R.G. and S.P. MARSH (1966), J. Geophys. Res., 71, 1751.

PRESS, F. (1968a), J. Geophys. Res., 73, 5223.

PRESS, F. (1968b), Science, 160, 1218.

PRESS, F. (1969), in press, Science.

RINGWOOD, A.E. (1969), this volume.

TOKSOZ, M.N. and D.L. ANDERSON (1966), J. Geophys. Res., 71, 1649.

WANG, C. (1969), in press, J. Geophys. Res.

WIGGINS, R.A. (1968), Phys. Earth Planetary Interiors, 1, 201.

WIGGINS, R.A. (1969), in preparation.

DIAGNOSTIC NUMBER 18
TIME SINCE LAST DIAGNOSTIC 191.61 SECONDS
TOTAL COMPUTATION TIME 3347.42 SECONDS

```
ALPHA SLMD                BETA SLMD                 RHO SLTMOD                VRPR
COUNT =        450        COUNT =       5025        COUNT =     531881        COUNT =    365916
AV TIME =0.00140          AV TIME =0.00192          AV TIME =0.00380          AV TIME =0.00085
TO TIME =     0.63        TO TIME =     9.65        TO TIME =2020.39          TO TIME =  310.52

                                                                              NUMB PASS =    11
                                                                              % PASSING = 8.53
                                                                              A B MODELS - 129
                                                                              R LOOPS TILL SUC
                                                                                  1- 300     1
                                                                                301- 600     0
                                                                                601- 900     4
                                                                                901-1200     2
                                                                               1201-1500     2
                                                                               1501-1800     1
                                                                               1801-2100     0
                                                                               2101-2400     1
                                                                               2401-2700     0
                                                                               2701-3000     0
                                                                              FAILED       118

ALPHA TTT                 BETA TTT                  MASMOM
% PASSING = 0.0           % PASSING =26.25          % PASSING =68.79
AV TIME =0.0              AV TIME =0.01588          AV TIME =0.00121
TO TIME =      0.0        TO TIME =    79.79        TO TIME = 642.28

ALPHA VRPR                BETA VRPR
% PASSING =*****          % PASSING = 9.78
AV TIME =*******          AV TIME =0.00667
TO TIME =     7.46        TO TIME =     8.80
```

RAYS TESTED	1	2	3	4	5	6	7	8	9	10	11	12	13	14	15	16	17	18	19	20
ALPHA TTT	0	0	0	0	0	0	0	0	0	0	0	0	0	0	0	0	0	0	0	0
BETA TTT	1561	1149	56	150	251	31	15	476	15	2	1319	0	0	0	0	0	0	0	0	0

THE PROGRAM STARTS AGAIN WITH A NEW CORE AFTER 150 ALPHA TTT FAILURES, OR 10 BETA TTT FAILURES, OR 3000 RHO VRPR FAILURES

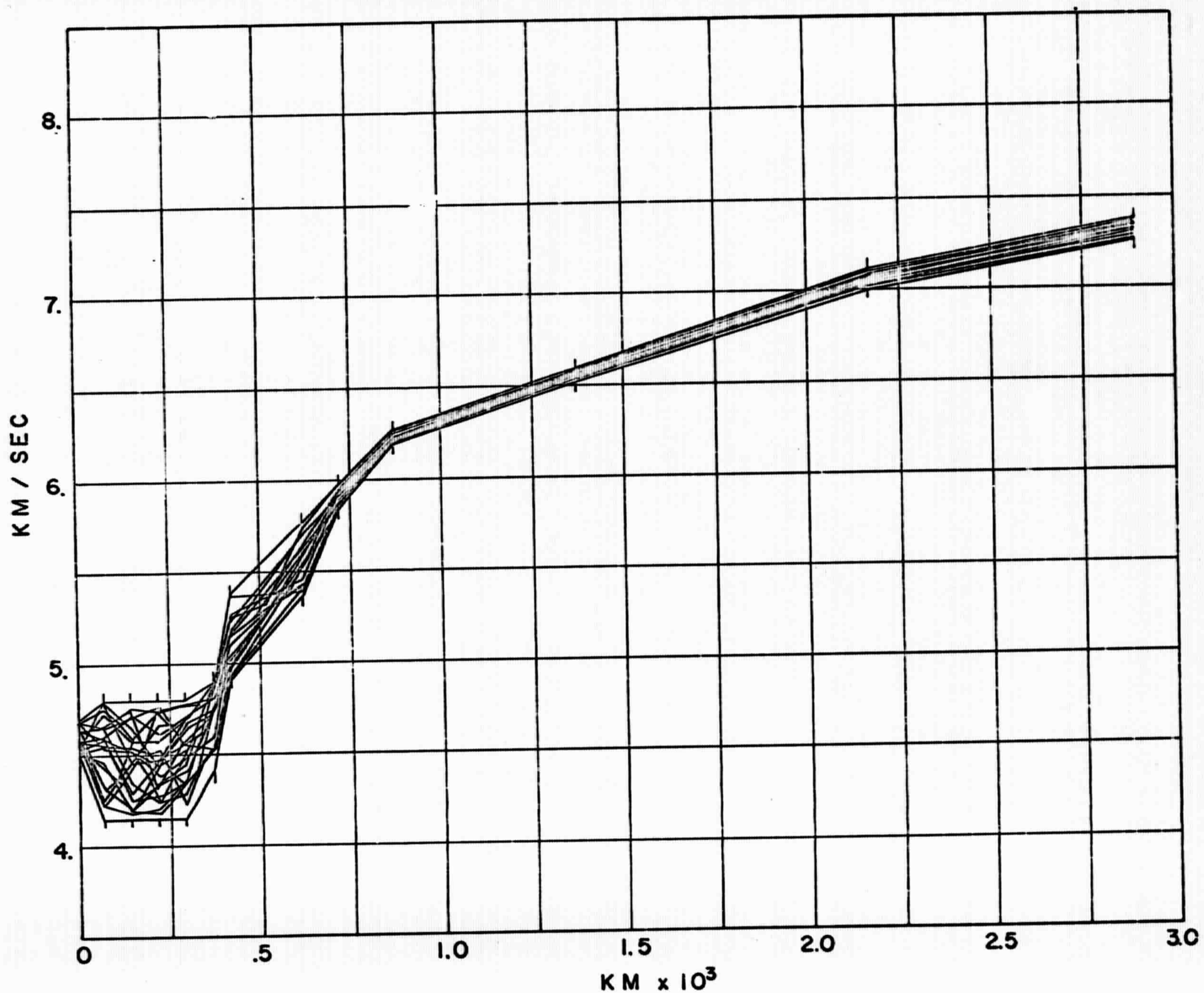
KM / SEC
8.
7.
6.
5.
4.
0
.5
1.0
1.5
2.0
2.5
3.0
KM x 10^3

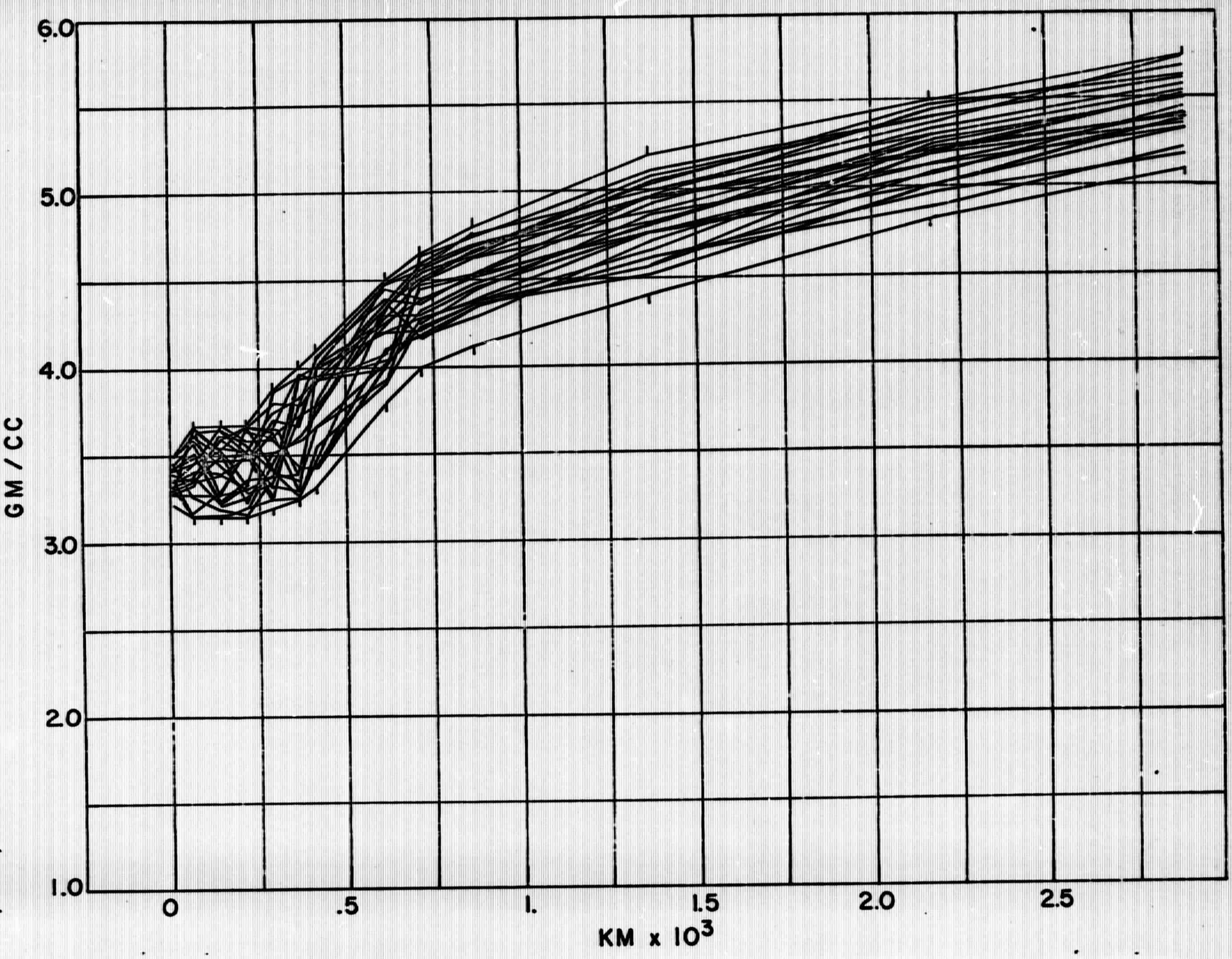

GM / CC
6.0
5.0
4.0
3.0
2.0
1.0
0
.5
1.
1.5
2.0
2.5
KM x 10^3

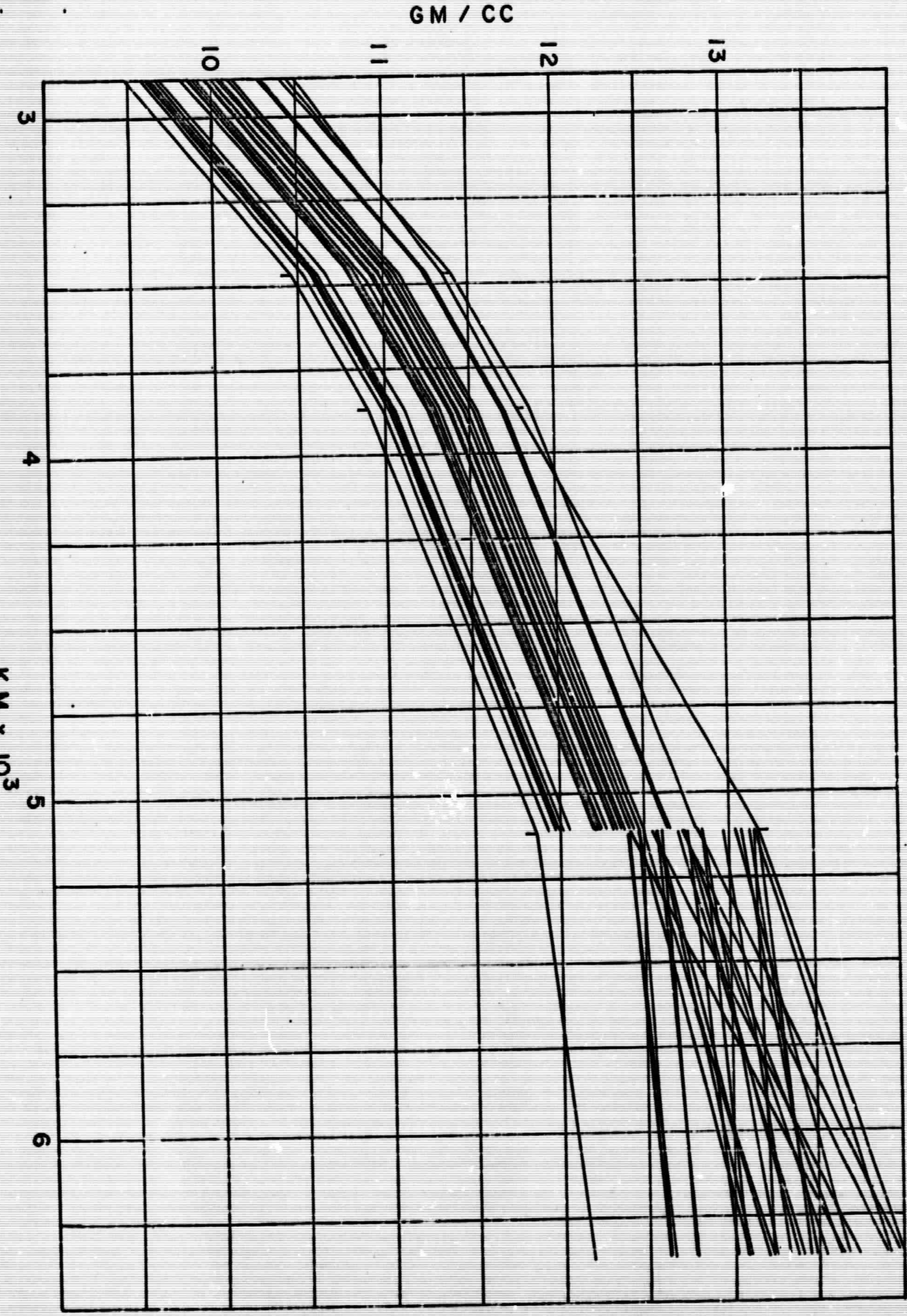

GM / CC
10
11
12
13
3
4
5
6
KM x 10^3

```
MODEL    1    MASS= 5.97600   I= 8.02400   I/MA2= 0.33080   M.C.D.= 11.1859   IC/MA2C= 0.38854
 0.0    0.0      937.70    935.80    1.90          16.6   24.22     579.83    575.59    4.23            15.5   32.49    713.51    709.28    4.23    A
14.4   47.02     931.97    926.75    5.22          13.3   55.22    1045.72   1039.71    6.01            12.2   65.22   1173.89   1168.21    5.68
11.1   72.63   1260.32   1256.00     4.32          10.0   83.69    1375.71   1374.27    1.44             8.9   94.14   1474.78   1470.89    3.89
 7.8   68.09   1264.38   1260.27     4.11
0 S       2 3221.5 -7.5      4 1543.4 -3.6      6  963.7 -0.2     14  449.3  0.9     30  261.8 -0.7     50  178.7  0.5     70  134.0 -0.2
          3 2129.6 -4.4      5 1189.4  0.4      7  813.0  1.3      8  709.2  1.6      9  635.7  1.7     10  581.4  1.4     11  538.9  1.4
       * 12  504.2  2.2     13  474.7  1.6     15  427.0  0.8     16  407.3  0.8     17  389.8  0.4     18  374.1  0.7     20  347.1 -0.3
         21  335.4 -0.4     22  324.7  0.7     24  305.7 -0.0     26  289.2 -0.2     28  274.7 -0.3     32  250.2 -0.6     34  239.6 -0.4
         36  229.9 -0.1     39  216.8  0.1     42  205.0  0.3     45  194.4  0.5     55  165.2  0.6     60  153.5  0.4     65  143.1 -0.1
         75  125.8 -0.5     19  360.0 -0.6
0 T       4 1308.4  4.4      8  738.2  1.2     11  575.9  0.2     40  201.1 -0.2     80  106.5  0.0     17  409.8  1.5      3 1708.5  0.5
          5 1079.3  3.3      6  928.5  3.1      7  820.3  2.4      9  673.2  1.2     10  620.1  0.7     15  452.3 -0.0     12  538.2  1.3
         13  505.7  1.0     14  477.3  0.3     16  429.9  0.3      2 2639.3 -0.7     18  391.7  1.5     19  375.2  0.7     20  360.1 -0.5    B
         21  346.2 -0.9     22  333.4 -0.9     23  321.6  0.1     25  300.3  0.1     27  281.7  0.1     30  257.8 -0.1     35  225.9 -0.3
         45  181.1 -0.2     50  164.7 -0.2     60  139.4 -0.1     70  120.8 -0.0     90   95.2  0.0    105   82.1  0.0
0 R       1 1226.7 -0.9
1 S       2 1473.5  1.5      3 1067.4  3.4   *  5  734.2  5.5      6  662.2  2.2      8  559.3  3.9   * 12  393.4 -3.4
1 T
1 R
2 S    *  2  921.8 16.3   *  4  730.7  5.8      6  595.9  1.3     10  415.9  0.7
2 T
2 R
 1 6371.0   1.52   0.0    1.03     2 6368.0   1.52   0.0    1.03*    3 6368.0   6.55   3.73   2.84     4 6361.0   6.55   3.73   2.84*
 5 6361.0   8.00   4.62   3.44     6 6338.0   8.06   4.58   3.48     7 6338.0   8.06   4.58   3.48     8 6318.0   8.11   4.53   3.53
 9 6300.0   8.16   4.50   3.56    10 6275.0   8.03   4.45   3.58    11 6250.0   7.89   4.41   3.60    12 6225.0   7.76   4.36   3.62
13 6200.0   8.00   4.36   3.59    14 6175.0   8.23   4.35   3.56    15 6150.0   8.47   4.34   3.53    16 6125.0   8.51   4.36   3.54
17 6100.0   8.54   4.38   3.55    18 6075.0   8.58   4.40   3.56    19 6050.0   8.61   4.51   3.55    20 6025.0   8.65   4.61   3.54
21 6000.0   8.68   4.71   3.53    22 5975.0   9.17   5.01   3.46    23 5950.0   9.67   5.31   3.39    24 5925.0   9.71   5.34   3.48
25 5900.0   9.75   5.37   3.57    26 5875.0   9.79   5.41   3.66    27 5850.0   9.83   5.44   3.75    28 5825.0   9.88   5.47   3.84
29 5800.0   9.92   5.50   3.93    30 5775.0   9.96   5.53   4.02    31 5750.0  10.00   5.56   4.11    32 5725.0  10.24   5.67   4.20
33 5700.0  10.48   5.77   4.29    34 5675.0  10.73   5.87   4.38    35 5650.0  10.97   5.98   4.47    36 5625.0  11.01   6.02   4.49
37 5600.0  11.05   6.06   4.50    38 5550.0  11.13   6.15   4.52    39 5500.0  11.21   6.23   4.55    40 5400.0  11.37   6.30   4.58
41 5300.0  11.53   6.37   4.62    42 5200.0  11.70   6.44   4.65    43 5100.0  11.86   6.50   4.68    44 5000.0  12.02   6.57   4.72    C
45 4800.0  12.27   6.69   4.79    46 4600.0  12.52   6.81   4.87    47 4400.0  12.78   6.94   4.95    48 4200.0  13.03   7.06   5.03
49 4000.0  13.23   7.12   5.12    50 3800.0  13.44   7.19   5.22    51 3700.0  13.54   7.22   5.27    52 3650.0  13.59   7.24   5.29
53 3600.0  13.64   7.25   5.32    54 3575.0  13.67   7.26   5.33    55 3550.0  13.70   7.27   5.34    56 3525.0  13.72   7.28   5.36
57 3500.0  13.75   7.28   5.37    58 3476.7  13.77   7.29   5.38    59 3476.7   7.96   0.0   10.08    60 3450.0   8.01   0.0   10.12
61 3425.0   8.05   0.0   10.16    62 3400.0   8.10   0.0   10.20    63 3350.0   8.19   0.0   10.28    64 3300.0   8.28   0.0   10.36
65 3100.0   8.64   0.0   10.69    66 2900.0   9.00   0.0   11.02    67 2700.0   9.30   0.0   11.24    68 2500.0   9.60   0.0   11.45
69 2300.0   9.69   0.0   11.60    70 2100.0   9.78   0.0   11.74    71 1900.0   9.86   0.0   11.89    72 1800.0   9.91   0.0   11.96
73 1700.0   9.95   0.0   12.03    74 1600.0  10.00   0.0   12.10    75 1500.0  10.04   0.0   12.17    76 1450.0  10.06   0.0   12.21
77 1400.0  10.09   0.0   12.25    78 1350.0  10.11   0.0   12.28    79 1300.0  10.13   0.0   12.32    80 1253.0  10.15   0.0   12.35
81 1253.0  11.15   0.0   12.88    82 1100.0  11.15   0.0   12.95    83  900.0  11.16   0.0   13.05    84  700.0  11.17   0.0   13.14
85  500.0  11.17   0.0   13.24    86  300.0  11.18   0.0   13.33    87  150.0  11.19   0.0   13.40    88    0.0  11.19   0.0   13.47
 4 ALPHA REVERSALS BEFORE LAYERS        10    13    59    63
 2 BETA REVERSALS BEFORE LAYERS        6    19
 2 RHO REVERSALS BEFORE LAYERS       22    24
       5     10.   22.6          23    421.   19.3           58   2898.   24.0
       9     71.   22.6          31    621.   23.0           59   2898.   54.8
      12    146.   23.9          35    721.   23.3           66   3471.   56.0       D
      15    221.   21.3          39    871.   23.6           68   3871.   56.2
      18    296.   21.3          44   1371.   23.2           80   5118.   58.8
      21    371.   21.4          48   2171.   23.4           81   5118.   58.2
                                           88   6371.   60.8
```

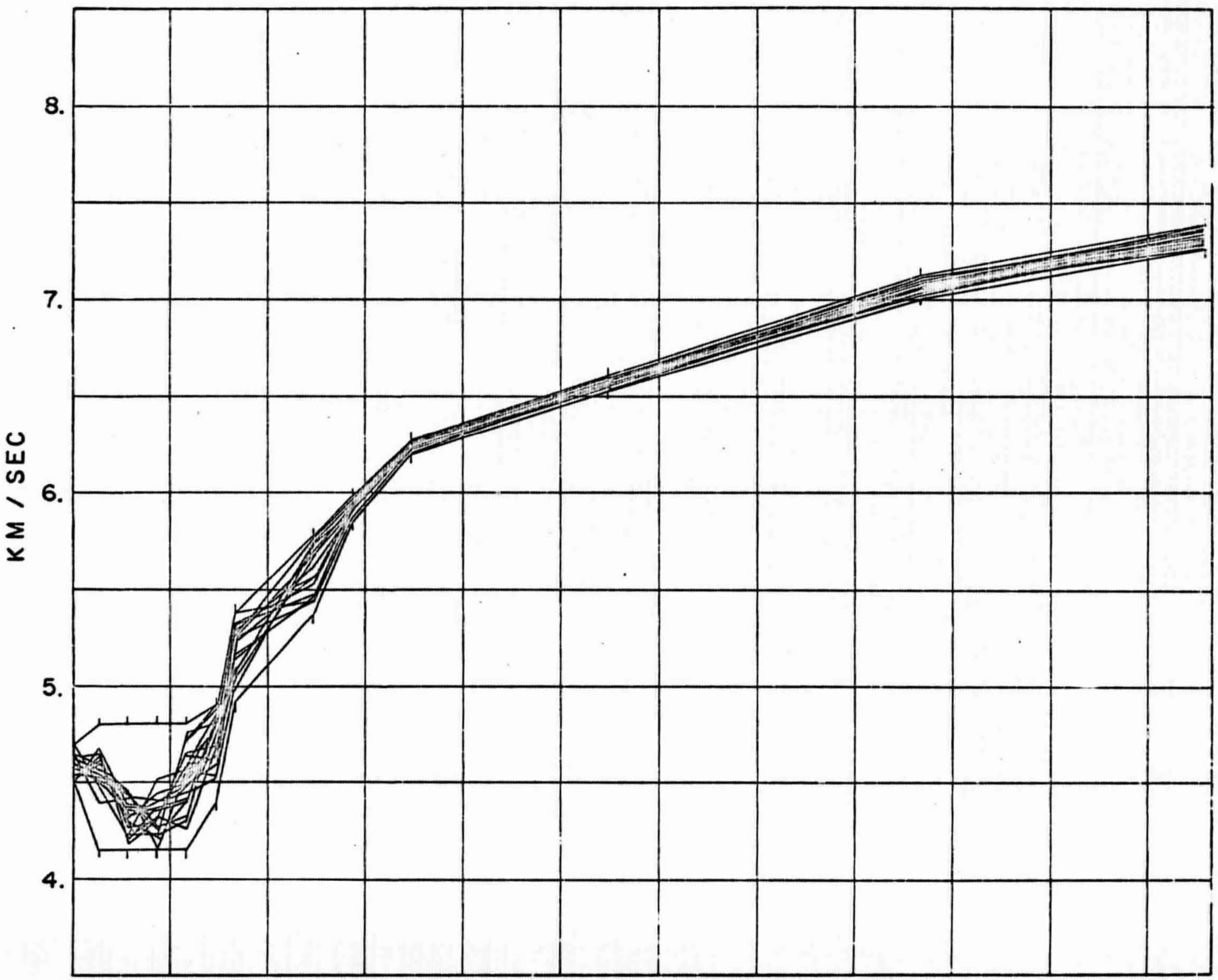
KM / SEC
8.
7.
6.
5.
4.
0
5
10
15
20
25
KM x 10²

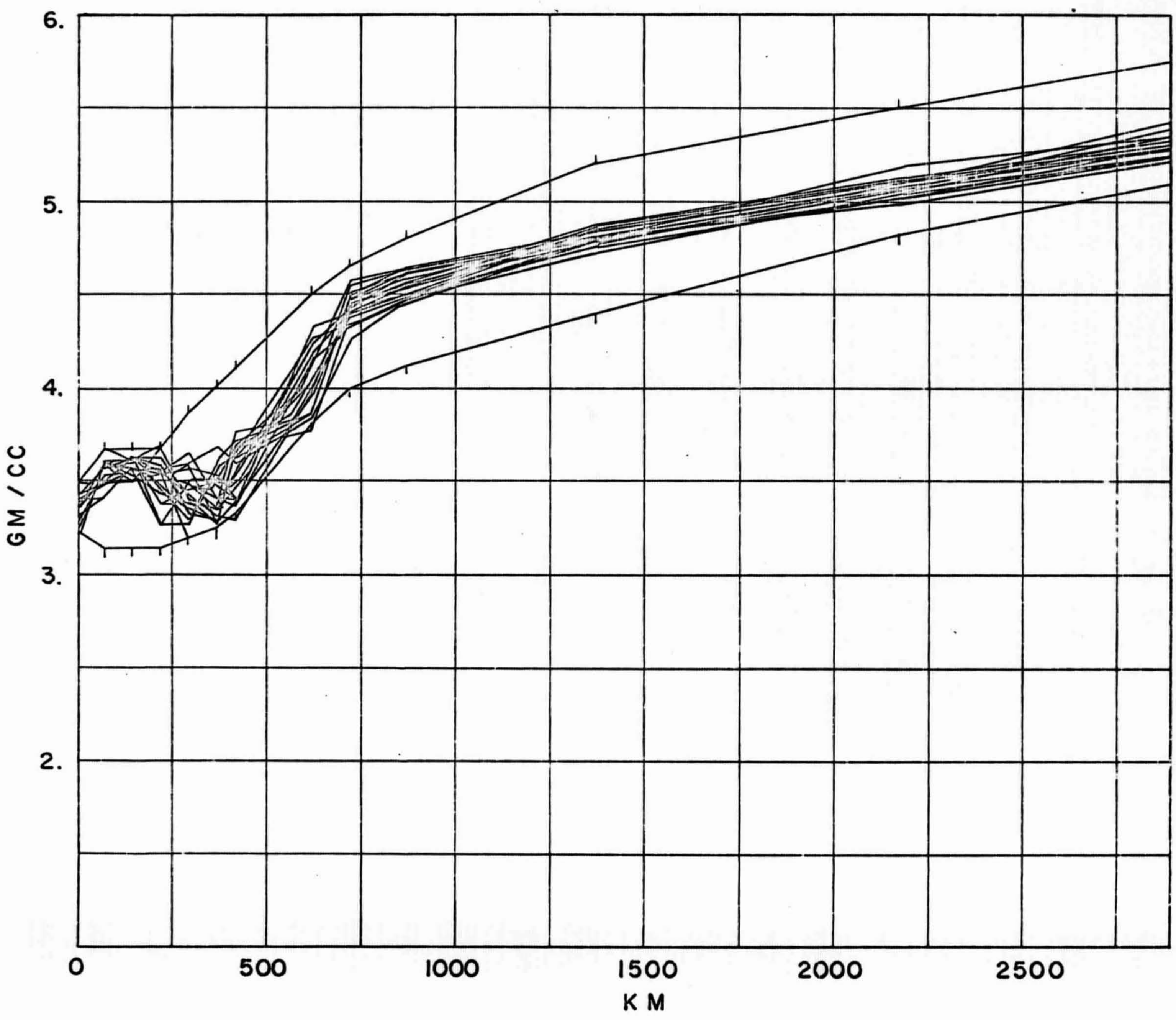

GM / CC
6.
5.
4.
3.
2.
0
500
1000
1500
2000
2500
K M

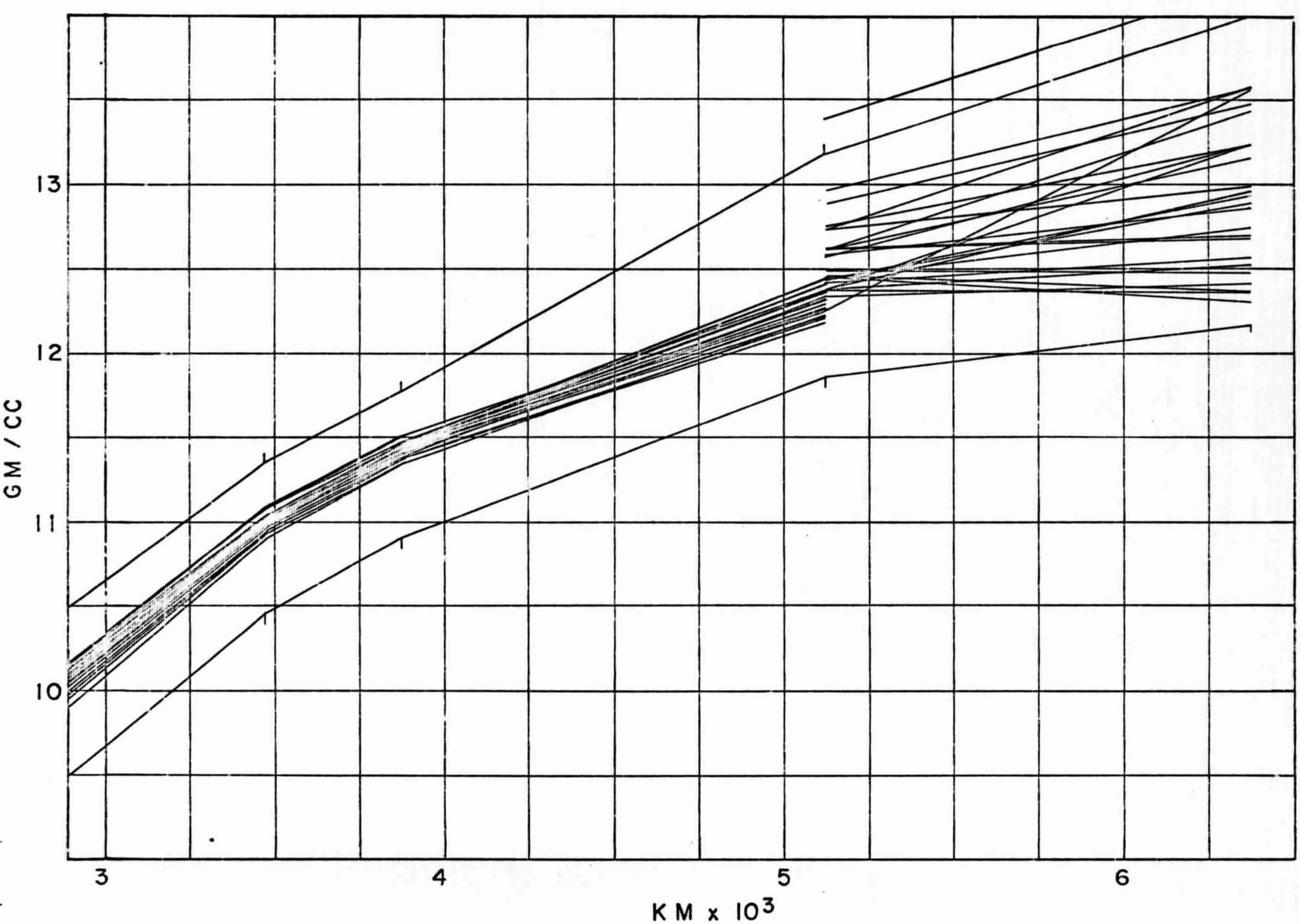
GM / CC
13
12
11
10
3
4
5
6
KM x 10^3

DEPTH	ALPHA	BETA	RHO	ϕ	K/μ	σ							
10.	8.000	4.595	3.462	35.8	1.79	0.254	10.	8.000	4.502	3.359	37.0	1.82	0.268
71.	8.160	4.499	3.559	39.7	1.97	0.293	71.	8.160	4.632	3.575	38.0	1.77	0.262
146.	7.760	4.373	3.634	34.7	1.82	0.267	146.	7.760	4.294	3.567	35.6	1.93	0.279
221.	8.470	4.248	3.370	47.7	2.64	0.332	221.	8.470	4.208	3.494	48.1	2.72	0.336
296.	8.580	4.501	3.457	45.5	2.16	0.299	296.	8.580	4.761	3.325	43.4	1.91	0.278
371.	8.680	4.834	3.489	44.2	1.89	0.275	371.	8.680	4.807	3.528	44.5	1.93	0.279
421.	9.670	5.255	3.491	59.4	2.33	0.312	421.	9.670	4.975	3.618	60.5	2.44	0.320
621.	10.000	5.734	4.168	56.2	1.71	0.255	621.	10.000	5.720	3.860	56.4	1.72	0.257
721.	10.970	5.893	4.414	74.2	2.14	0.299	721.	10.970	5.905	4.439	73.8	2.12	0.296
871.	11.210	6.222	4.496	74.0	1.91	0.277	871.	11.210	6.227	4.615	74.0	1.91	0.277
1371.	12.020	6.576	4.753	86.8	2.01	0.286	1371.	12.020	6.572	4.795	86.9	2.01	0.287
2171.	13.030	7.040	5.117	103.7	2.09	0.294	2171.	13.030	7.040	5.036	103.7	2.09	0.294
2898.	13.770	7.346	5.253	117.7	2.18	0.301	2898.	13.770	7.288	5.374	118.8	2.24	0.305
2898.	7.960	0.0	10.138				2898.	7.960	0.0	10.097			
3471.	9.000	0.0	11.036				3471.	9.000	0.0	11.004			
3871.	9.600	0.0	11.446				3871.	9.600	0.0	11.423			
5118.	10.150	0.0	12.272				5118.	10.150	0.0	12.298			
5118.	11.150	0.0	12.429	1.07			5118.	11.150	0.0	12.382	6.92		
6371.	11.190	0.0	12.893				6371.	11.190	0.0	12.523			
10.	8.000	4.510	3.482	36.9	1.81	0.267	10.	8.000	4.576	3.349	36.1	1.72	0.257
71.	8.160	4.613	3.493	38.2	1.80	0.265	71.	8.160	4.488	3.563	39.7	1.97	0.283
146.	7.760	4.329	3.610	35.7	1.89	0.274	146.	7.760	4.446	3.593	33.9	1.71	0.256
221.	8.470	4.369	3.461	46.5	2.46	0.321	221.	8.470	4.238	3.370	47.9	2.66	0.333
296.	8.580	4.476	3.293	46.9	2.34	0.313	296.	8.580	4.538	3.394	46.2	2.24	0.306
371.	8.680	4.703	3.606	45.0	2.07	0.292	371.	8.680	4.974	3.277	43.7	1.94	0.279
421.	9.670	5.080	3.714	59.1	2.29	0.309	421.	9.670	5.058	3.672	59.4	[illegible]	0.312
621.	10.000	5.755	3.857	55.8	1.69	0.252	621.	10.000	5.654	3.938	57.4	1.79	0.265
721.	10.970	5.878	4.315	74.3	2.15	0.299	721.	10.970	5.907	4.441	73.8	2.12	0.296
871.	11.210	6.236	4.502	73.8	1.90	0.276	871.	11.210	6.199	4.536	74.4	1.94	0.280
1371.	12.020	6.598	4.856	86.4	1.99	0.284	1371.	12.020	6.573	4.835	86.9	2.01	0.287
2171.	13.030	7.050	5.192	103.5	2.08	0.293	2171.	13.030	7.053	5.119	103.5	2.08	0.293
2898.	13.770	7.262	5.311	119.3	2.26	0.307	2898.	13.770	7.307	5.294	118.4	2.22	0.304
2898.	7.960	0.0	10.067				2898.	7.960	0.0	10.057			
3471.	9.000	0.0	10.967				3471.	9.000	0.0	10.977			
3871.	9.600	0.0	11.374				3871.	9.600	0.0	11.329			
5118.	10.150	0.0	12.182				5118.	10.150	0.0	12.259			
5118.	11.150	0.0	12.609	5.18			5118.	11.150	0.0	12.338	3.62		
6371.	11.190	0.0	13.432				6371.	11.190	0.0	12.415			
10.	8.000	4.628	3.359	35.4	1.65	0.249	10.	8.000	4.526	3.400	36.7	1.79	0.265
71.	8.150	4.389	3.620	40.9	2.12	0.297	71.	8.160	4.685	3.474	37.3	1.70	0.254
146.	7.750	4.422	3.523	34.1	1.75	0.260	146.	7.760	4.175	3.493	37.0	2.12	0.296
221.	8.470	4.397	3.424	46.0	2.38	0.316	221.	8.470	4.313	3.666	46.9	2.52	0.325
296.	8.580	4.484	3.374	46.8	2.33	0.312	296.	8.580	4.637	3.396	44.9	2.09	0.294
371.	8.630	4.60[illegible]	3.338	47.1	2.22	0.304	371.	8.680	4.613	3.406	47.0	2.21	0.303
421.	9.670	5.210	3.535	57.3	2.11	0.295	421.	9.670	5.374	3.302	55.0	1.90	0.277
621.	10.000	5.655	4.124	57.4	1.79	0.265	621.	10.000	5.440	3.984	60.5	2.25	0.290
721.	10.970	5.906	4.456	73.8	2.12	0.296	721.	10.970	5.940	4.542	74.9	2.20	0.302
871.	11.210	6.193	4.593	74.5	1.94	0.280	871.	11.210	6.243	4.632	73.7	1.89	0.275
1371.	12.020	6.597	4.786	86.6	2.00	0.285	1371.	12.020	6.554	4.790	97.2	2.03	0.298
2171.	13.030	7.039	5.066	103.7	2.09	0.294	2171.	13.030	7.033	5.057	103.8	2.19	0.294
2898.	13.770	7.342	5.139	117.3	2.17	0.300	2898.	13.770	7.333	5.241	117.9	2.19	0.302
2898.	7.950	0.0	10.097				2898.	7.960	0.0	10.133			
3471.	9.000	0.0	11.033				3471.	9.000	0.0	11.020			
3871.	9.630	0.0	11.466				3871.	9.600	0.0	11.419			
5118.	10.150	0.0	12.362				5118.	10.150	0.0	12.205			
5118.	11.150	0.0	12.392	3.15			5118.	11.150	0.0	12.567	7.48		
6371.	11.190	0.0	12.958				6371.	11.190	0.0	13.222			

10.	8.000	4.533	3.245	36.6	1.78	0.264
71.	8.160	4.585	3.591	38.6	1.83	0.269
146.	7.760	4.438	3.550	34.0	1.72	0.257
221.	8.470	4.224	3.556	48.0	2.69	0.334
296.	8.580	4.292	3.593	49.1	2.66	0.333
371.	8.680	4.889	3.681	43.5	1.82	0.268
421.	9.670	5.230	3.590	57.0	2.09	0.293
621.	10.000	5.689	3.838	56.8	1.76	0.261
721.	10.970	5.965	4.255	72.9	2.05	0.290
871.	11.210	6.265	4.461	73.3	1.87	0.273
1371.	12.020	6.571	4.962	96.9	2.01	0.287
2171.	13.030	7.057	5.116	103.4	2.08	0.292
2898.	13.770	7.277	5.272	119.0	2.25	0.306
2898.	7.960	0.0	10.000			
3471.	9.000	0.0	10.945			
3871.	9.600	0.0	11.389			
5118.	10.150	0.0	12.330	6.42		
5118.	11.150	0.0	12.749			
6371.	11.190	0.0	13.231			

10.	8.000	4.490	3.271	37.1	1.84	0.270
71.	8.160	4.585	3.572	38.6	1.93	0.269
146.	7.760	4.451	3.533	33.8	1.71	0.255
221.	8.470	4.209	3.498	48.1	2.72	0.336
296.	8.580	4.412	3.504	47.7	2.45	0.320
371.	8.680	4.947	3.398	44.0	1.87	0.273
421.	9.670	5.124	3.592	58.5	2.23	0.305
621.	10.000	5.673	4.036	57.1	1.77	0.263
721.	10.970	5.930	4.446	73.5	2.09	0.294
871.	11.210	6.207	4.548	74.3	1.93	0.279
1371.	12.020	6.589	4.767	86.6	1.99	0.285
2171.	13.030	7.078	5.053	103.0	2.06	0.291
2898.	13.770	7.270	5.390	119.1	2.25	0.307
2898.	7.960	0.0	10.087			
3471.	9.000	0.0	11.003			
3871.	9.600	0.0	11.424			
5118.	10.150	0.0	12.285	6.21		
5118.	11.150	0.0	12.450			
6371.	11.190	0.0	12.745			

10.	8.000	4.482	3.281	37.2	1.85	0.271
71.	8.160	4.645	3.597	37.6	1.75	0.260
146.	7.760	4.260	3.632	36.0	1.98	0.284
221.	8.470	4.313	3.624	46.9	2.52	0.325
296.	8.580	4.445	3.365	47.3	2.39	0.317
371.	8.680	4.893	3.357	43.4	1.81	0.267
421.	9.670	5.291	3.426	56.2	2.01	0.286
621.	10.000	5.550	3.953	58.9	1.91	0.277
721.	10.970	5.960	4.384	73.0	2.05	0.291
871.	11.210	6.201	4.544	74.4	1.93	0.280
1371.	12.020	6.571	4.821	86.9	2.01	0.287
2171.	13.030	7.051	5.109	103.5	2.09	0.293
2898.	13.770	7.362	5.244	117.3	2.17	0.300
2898.	7.960	0.0	10.135			
3471.	9.000	0.0	11.029			
3871.	9.600	0.0	11.428			
5118.	10.150	0.0	12.711	3.38		
5118.	11.150	0.0	12.370			
6371.	11.190	0.0	12.353			

10.	8.000	4.529	3.354	36.7	1.79	0.264
71.	8.160	4.520	3.571	39.3	1.93	0.279
146.	7.760	4.308	3.545	35.5	1.91	0.277
221.	8.470	4.439	3.533	45.5	2.31	0.311
296.	8.580	4.494	3.404	46.7	2.31	0.311
371.	8.680	4.698	3.299	45.9	2.08	0.293
421.	9.670	5.229	3.286	57.1	2.09	0.293
621.	10.000	5.641	3.980	57.6	1.81	0.267
721.	10.970	5.874	4.561	74.3	2.15	0.299
871.	11.210	6.212	4.640	74.2	1.92	0.278
1371.	12.020	6.541	4.832	87.4	2.04	0.290
2171.	13.030	7.052	5.088	103.5	2.08	0.293
2898.	13.770	7.336	5.324	117.9	2.12	0.302
2898.	7.960	0.0	10.027			
3471.	9.000	0.0	10.940			
3871.	9.600	0.0	11.361			
5118.	10.150	0.0	12.226	5.04		
5118.	11.150	0.0	12.730			
6371.	11.190	0.0	12.986			

10.	8.000	4.560	3.298	36.3	1.74	0.259
71.	8.160	4.533	3.610	39.2	1.91	0.277
146.	7.760	4.427	3.609	34.1	1.74	0.259
221.	8.470	4.247	3.690	47.7	2.64	0.332
296.	8.580	4.520	3.318	46.4	2.27	0.308
371.	8.690	4.781	3.366	44.9	1.96	0.282
421.	9.670	5.226	3.555	57.1	2.09	0.294
621.	10.000	5.541	4.195	59.1	1.92	0.278
721.	10.970	5.951	4.403	73.1	2.06	0.291
871.	11.210	6.256	4.521	73.5	1.88	0.274
1371.	12.020	6.588	4.746	86.6	2.00	0.285
2171.	13.030	7.037	5.019	103.8	2.10	0.294
2898.	13.770	7.307	5.294	118.4	2.22	0.304
2898.	7.960	0.0	10.168			
3471.	9.000	0.0	11.088			
3871.	9.600	0.0	11.505			
5118.	10.150	0.0	12.336	-2.37		
5118.	11.150	0.0	12.611			
6371.	11.190	0.0	13.158			

10.	8.000	4.683	3.321	34.8	1.58	0.239
71.	8.160	4.504	3.400	39.5	1.95	0.281
146.	7.760	4.424	3.589	34.1	1.74	0.259
221.	8.470	4.265	3.551	47.5	2.61	0.330
296.	8.580	4.376	3.436	48.7	2.60	0.330
371.	8.680	4.931	3.469	44.2	1.89	0.276
421.	9.670	5.223	3.393	57.1	2.09	0.294
621.	10.000	5.550	4.117	58.9	1.91	0.277
721.	10.970	5.914	4.569	73.7	2.11	0.295
871.	11.210	6.206	4.626	74.3	1.93	0.279
1371.	12.020	6.570	4.812	86.9	2.01	0.287
2171.	13.030	7.106	4.973	102.5	2.03	0.288
2898.	13.770	7.311	5.230	118.3	2.21	0.304
2898.	7.960	0.0	9.976			
3471.	9.000	0.0	10.968			
3871.	9.600	0.0	11.437			
5118.	10.150	0.0	12.440	4.03		
5118.	11.150	0.0	13.292			
6371.	11.190	0.0	14.186			

10.	8.000	4.623	3.436	35.5	1.66	0.249
71.	8.160	4.498	3.562	39.6	1.96	0.282
146.	7.760	4.363	3.618	34.8	1.83	0.269
221.	8.470	4.343	3.532	46.6	2.47	0.322
296.	8.580	4.403	3.565	47.8	2.46	0.321
371.	8.680	4.712	3.525	45.7	2.06	0.291
421.	9.670	5.312	3.395	55.9	1.98	0.284
621.	10.000	5.561	4.110	58.8	1.90	0.276
721.	10.970	5.979	4.473	72.7	2.03	0.289
871.	11.210	6.232	4.549	73.9	1.90	0.276
1371.	12.920	6.573	4.717	86.9	2.01	0.287
2171.	13.030	7.056	5.029	103.4	2.08	0.293
2898.	13.770	7.292	5.378	118.7	2.23	0.305
2898.	7.960	0.0	10.075			
3471.	9.000	0.0	11.018			
3871.	9.600	0.0	11.453			
5118.	10.150	0.0	12.352			
5118.	11.150	0.0	12.882			
6371.	11.190	0.0	13.472			

3.75

10.	8.000	4.628	3.394	35.4	1.65	0.249
71.	8.160	4.486	3.589	39.8	1.99	0.283
146.	7.760	4.391	3.565	34.6	1.80	0.266
221.	8.470	4.363	3.259	46.4	2.44	0.319
296.	8.580	4.548	3.266	46.0	2.23	0.306
371.	8.680	4.696	3.572	45.9	2.09	0.293
421.	9.670	5.159	3.644	58.0	2.18	0.301
621.	10.000	5.445	4.266	60.5	2.04	0.289
721.	10.970	5.942	4.337	73.3	2.07	0.292
871.	11.210	6.236	4.444	73.8	1.90	0.276
1371.	12.920	6.589	4.803	86.6	1.99	0.285
2171.	13.030	7.042	5.108	103.7	2.09	0.294
2898.	13.770	7.334	5.271	117.9	2.19	0.302
2898.	7.960	0.0	10.110			
3471.	9.000	0.0	11.017			
3871.	9.600	0.0	11.427			
5118.	10.150	0.0	12.241			
5118.	11.150	0.0	12.435			
6371.	11.190	0.0	12.936			

1.52

10.	8.000	4.506	3.395	36.9	1.82	0.268
71.	8.160	4.469	3.400	37.5	1.72	0.257
146.	7.760	4.353	3.572	35.0	1.84	0.270
221.	8.470	4.313	3.544	46.9	2.52	0.325
296.	8.580	4.252	3.649	49.5	2.74	0.337
371.	8.680	4.677	3.303	46.2	2.11	0.295
421.	9.670	5.269	3.491	56.5	2.03	0.289
621.	10.000	5.735	4.120	56.1	1.71	0.255
721.	10.970	5.858	4.319	74.6	2.17	0.301
871.	11.210	6.197	4.467	74.5	1.94	0.280
1371.	12.920	6.585	4.772	86.7	2.00	0.286
2171.	13.030	7.067	5.182	103.2	2.07	0.292
2898.	13.770	7.271	5.345	119.1	2.25	0.307
2898.	7.960	0.0	9.970			
3471.	9.000	0.0	10.932			
3871.	9.600	0.0	11.382			
5118.	10.150	0.0	12.332			
5118.	11.150	0.0	12.418			
6371.	11.190	0.0	12.564			

7.77

10.	8.000	4.522	3.355	36.7	1.80	0.265
71.	8.160	4.594	3.595	38.4	1.82	0.269
146.	7.760	4.225	3.519	36.4	2.04	0.289
221.	8.470	4.231	3.520	47.9	2.67	0.334
296.	8.580	4.725	3.417	43.8	1.96	0.282
371.	8.680	4.984	3.261	43.5	1.83	0.269
421.	9.670	5.246	3.547	56.8	2.06	0.291
621.	10.000	5.430	3.918	60.7	2.06	0.291
721.	10.970	5.880	4.507	74.1	2.14	0.298
871.	11.210	6.264	4.604	73.3	1.97	0.273
1371.	12.920	6.587	4.803	86.6	2.00	0.285
2171.	13.030	7.050	5.031	103.5	2.08	0.293
2898.	13.770	7.350	5.266	117.6	2.18	0.301
2898.	7.960	0.0	10.076			
3471.	9.000	0.0	10.996			
3871.	9.600	0.0	11.402			
5118.	10.150	0.0	12.244			
5118.	11.150	0.0	12.556			
6371.	11.190	0.0	13.229			

5.08

10.	8.000	4.610	3.359	35.7	1.68	0.251
71.	8.160	4.501	3.482	39.6	1.95	0.281
146.	7.760	4.226	3.563	36.4	2.04	0.289
221.	8.470	4.513	3.547	44.6	2.19	0.302
296.	8.580	4.553	3.316	45.9	2.20	0.303
371.	8.680	4.443	3.291	46.6	2.16	0.300
421.	9.670	5.026	3.396	59.8	2.37	0.315
621.	10.000	5.672	4.322	57.1	1.77	0.263
721.	10.970	5.952	4.395	73.1	2.06	0.291
871.	11.210	6.240	4.552	73.6	1.88	0.275
1371.	12.920	6.575	4.307	86.8	2.01	0.287
2171.	13.030	7.036	5.093	103.9	2.10	0.294
2898.	13.770	7.355	5.295	117.5	2.17	0.300
2898.	7.960	0.0	9.897			
3471.	9.000	0.0	10.898			
3871.	9.600	0.0	11.377			
5118.	10.150	0.0	12.423			
5118.	11.150	0.0	12.963			
6371.	11.190	0.0	13.566			

9.82

10.	8.000	4.639	3.213	35.3	1.64	0.247
71.	8.160	4.593	3.594	38.5	1.82	0.269
146.	7.760	4.225	3.581	36.4	2.04	0.289
221.	8.470	4.229	3.508	47.9	2.68	0.334
296.	8.580	4.717	3.337	43.9	1.99	0.283
371.	8.680	4.955	3.281	43.9	1.86	0.272
421.	9.670	5.141	3.636	58.3	2.20	0.303
621.	10.000	5.459	3.927	60.3	2.02	0.289
721.	10.970	5.933	4.424	73.3	2.08	0.293
871.	11.210	6.236	4.640	73.8	1.90	0.275
1371.	12.920	6.585	4.908	86.7	2.00	0.286
2171.	13.030	7.022	5.028	104.1	2.11	0.296
2898.	13.770	7.356	5.235	117.5	2.17	0.300
2898.	7.960	0.0	10.136			
3471.	9.000	0.0	11.042			
3871.	9.600	0.0	11.459			
5118.	10.150	0.0	12.309			
5118.	11.150	0.0	12.619			
6371.	11.190	0.0	12.624			

-2.03

10.	8.000	4.576	3.412	36.1	1.72	0.257
71.	8.160	4.534	3.491	39.2	1.91	0.277
146.	7.760	4.311	3.621	35.4	1.91	0.277
221.	8.470	4.376	3.263	46.2	2.41	0.318
296.	8.580	4.556	3.504	45.3	2.21	0.304
371.	8.680	4.527	3.593	48.0	2.34	0.313
421.	9.670	5.208	3.476	57.3	2.11	0.296
621.	10.000	5.622	4.145	57.9	1.83	0.269
721.	10.970	5.869	4.332	74.6	2.17	0.300
871.	11.210	6.263	4.488	73.4	1.87	0.273
1371.	12.020	6.597	4.869	86.5	1.99	0.284
2171.	13.030	7.029	5.107	103.9	2.10	0.295
2898.	13.770	7.375	5.264	117.1	2.15	0.299
2898.	7.960	0.0	9.956			
3471.	9.000	0.0	10.925			
3871.	9.600	0.0	11.379			
5118.	10.150	0.0	12.334			
5118.	11.150	0.0	12.723			
6371.	11.190	0.0	13.577			

5.70

10.	8.000	4.530	3.222	36.6	1.79	0.264
71.	8.160	4.499	3.575	39.6	1.96	0.282
146.	7.760	4.343	3.492	35.1	1.96	0.272
221.	8.470	4.350	3.472	46.5	2.46	0.321
296.	8.580	4.593	3.446	45.4	2.15	0.299
371.	8.680	4.620	3.408	46.9	2.20	0.302
421.	9.670	5.070	3.355	59.2	2.30	0.310
621.	10.000	5.701	4.220	56.7	1.74	0.250
721.	10.970	5.914	4.415	73.7	2.11	0.295
871.	11.210	6.258	4.605	73.4	1.88	0.274
1371.	12.020	6.521	4.775	87.9	2.06	0.291
2171.	13.030	7.085	5.098	102.9	2.05	0.290
2898.	13.770	7.340	5.293	117.8	2.19	0.302
2898.	7.960	0.0	10.031			
3471.	9.000	0.0	10.965			
3871.	9.600	0.0	11.403			
5118.	10.150	0.0	12.325			
5118.	11.150	0.0	12.374			
6371.	11.190	0.0	13.236			

7.43

10.	8.000	4.587	3.432	35.9	1.71	0.255
71.	8.160	4.504	3.464	39.5	1.95	0.281
146.	7.760	4.338	3.620	35.1	1.87	0.273
221.	8.470	4.345	3.579	46.6	2.47	0.321
296.	8.580	4.522	3.366	46.4	2.27	0.308
371.	8.680	4.693	3.335	46.1	2.10	0.295
421.	9.670	5.[illegible]88	3.522	59.0	2.28	0.309
621.	10.000	5.[illegible]59	4.092	55.8	1.68	0.252
721.	10.970	5.951	4.366	73.1	2.06	0.291
871.	11.210	6.231	4.487	73.9	1.90	0.276
1371.	12.020	6.559	4.862	87.1	2.03	0.288
2171.	13.030	7.052	5.054	103.5	2.08	0.293
2898.	13.770	7.371	5.242	117.2	2.16	0.299
2898.	7.960	0.0	10.150			
3471.	9.000	0.0	11.037			
3871.	9.600	0.0	11.436			
5118.	10.150	0.0	12.219			
5118.	11.150	0.0	12.459			
6371.	11.190	0.0	12.361			

6.17

10.	8.000	4.573	3.345	36.1	1.73	0.257
71.	8.160	4.540	3.611	39.1	1.90	0.276
146.	7.760	4.285	3.617	35.7	1.95	0.281
221.	8.470	4.243	3.503	47.7	2.65	0.332
296.	8.580	4.733	3.478	43.7	1.95	0.281
371.	8.680	4.822	3.348	44.3	1.91	0.277
421.	9.670	5.081	3.449	59.1	2.29	0.309
621.	10.000	5.694	4.012	56.8	1.75	0.260
721.	10.970	5.921	4.435	73.6	2.10	0.294
871.	11.210	6.195	4.563	74.5	1.94	0.280
1371.	12.020	6.600	4.802	86.4	1.98	0.286
2171.	13.030	7.005	5.047	104.4	2.13	0.297
2898.	13.770	7.373	5.398	117.1	2.15	0.299
2898.	7.960	0.0	10.087			
3471.	9.000	0.0	11.002			
3871.	9.600	0.0	11.424			
5118.	10.150	0.0	12.291			
5118.	11.150	0.0	12.443			
6371.	11.190	0.0	12.872			

1.64

10.	8.000	4.517	3.247	36.8	1.80	0.266
71.	8.160	4.612	3.514	38.2	1.80	0.265
146.	7.760	4.216	3.614	36.5	2.05	0.291
221.	8.470	4.301	3.532	47.1	2.54	0.326
296.	8.580	4.656	3.189	44.7	2.06	0.291
371.	8.680	4.689	3.237	46.0	2.09	0.294
421.	9.670	5.306	3.619	56.0	1.99	0.285
621.	10.000	5.467	4.014	60.1	2.01	0.287
721.	10.970	5.849	4.397	74.7	2.18	0.301
871.	11.210	6.235	4.555	73.8	1.90	0.276
1371.	12.020	6.590	4.864	86.6	1.99	0.285
2171.	13.030	7.050	5.096	103.5	2.08	0.293
2898.	13.770	7.319	5.422	118.2	2.21	0.303
2898.	7.960	0.0	9.979			
3471.	9.000	0.0	10.928			
3871.	9.600	0.0	11.338			
5118.	10.150	0.0	12.227			
5118.	11.150	0.0	12.244			
6371.	11.190	0.0	13.557			

10.33

10.	8.000	4.675	3.437	35.5	1.66	0.249
71.	8.160	4.647	3.466	37.9	1.75	0.260
146.	7.760	4.191	3.567	36.8	2.00	0.294
221.	8.470	4.384	3.578	46.1	2.40	0.317
296.	8.580	4.424	3.342	47.5	2.43	0.319
371.	8.680	4.860	3.474	43.8	1.86	0.272
421.	9.670	5.281	3.671	56.3	2.02	0.287
621.	10.000	5.416	3.866	60.9	2.09	0.292
721.	10.970	5.958	4.465	73.0	2.06	0.291
871.	11.210	6.212	4.571	74.2	1.92	0.278
1371.	12.020	6.549	4.792	87.3	2.04	0.289
2171.	13.030	7.101	5.070	102.5	2.03	0.289
2898.	13.770	7.349	5.293	117.6	2.19	0.301
2899.	7.960	0.0	10.005			
3471.	9.000	0.0	10.973			
3871.	9.600	0.0	11.430			
5118.	10.150	0.0	12.404			
5118.	11.150	0.0	12.613			
6371.	11.190	0.0	12.583			

9.71

10.	8.000	4.610	3.353	35.7	1.68	0.251
71.	8.160	4.558	3.527	38.9	1.87	0.273
146.	7.760	4.428	3.559	34.1	1.74	0.259
221.	8.470	4.151	3.580	48.8	2.83	0.342
296.	8.580	4.594	3.323	45.5	2.15	0.299
371.	8.680	4.770	3.382	45.0	1.98	0.284
421.	9.670	5.050	3.762	59.5	2.33	0.312
621.	10.000	5.740	3.849	56.1	1.70	0.254
721.	10.970	5.930	4.471	73.5	2.09	0.294
871.	11.210	6.253	4.607	73.5	1.88	0.274
1371.	12.020	6.545	4.799	87.4	2.04	0.289
2171.	13.030	7.025	5.007	104.0	2.11	0.295
2898.	13.770	7.377	5.238	117.1	2.15	0.299
2898.	7.960	0.0	10.155			
3471.	9.000	0.0	11.076			
3871.	9.600	0.0	11.501			
5118.	10.150	0.0	12.373		-3.41	
5118.	11.150	0.0	12.483			
6371.	11.190	0.0	12.471			

10.	8.000	4.552	3.514	36.4	1.76	0.261
71.	8.160	4.536	3.659	39.2	1.90	0.276
146.	7.760	4.332	3.598	35.2	1.89	0.274
221.	8.470	4.377	3.572	46.2	2.41	0.318
296.	8.580	4.413	3.373	47.7	2.45	0.320
371.	8.680	4.840	3.477	44.1	1.88	0.274
421.	9.670	5.318	3.684	55.8	1.97	0.283
621.	10.000	5.515	4.041	59.4	1.95	0.281
721.	10.970	5.933	4.308	73.4	2.09	0.293
871.	11.210	6.263	4.470	73.4	1.87	0.273
1371.	12.020	6.587	4.718	86.6	2.00	0.285
2171.	13.030	7.048	5.086	103.5	2.08	0.293
2898.	13.770	7.343	5.341	117.7	2.18	0.301
2898.	7.960	0.0	10.182			
3471.	9.000	0.0	11.076			
3871.	9.600	0.0	11.476			
5118.	10.150	0.0	12.261		3.33	
5118.	11.150	0.0	12.449			
6371.	11.190	0.0	12.300			

10.	8.000	4.601	3.289	35.8	1.69	0.253
71.	8.160	4.557	3.542	38.9	1.87	0.273
146.	7.760	4.316	3.513	35.4	1.90	0.276
221.	8.470	4.402	3.515	45.9	2.37	0.315
296.	8.580	4.451	3.583	47.2	2.38	0.316
371.	8.680	4.522	3.274	48.1	2.35	0.314
421.	9.670	5.252	3.686	56.7	2.06	0.291
621.	10.000	5.660	3.769	57.3	1.79	0.264
721.	10.970	5.891	4.484	74.1	2.13	0.297
871.	11.210	6.202	4.644	74.4	1.93	0.279
1371.	12.020	6.598	4.807	86.4	1.99	0.284
2171.	13.030	7.047	5.051	103.6	2.09	0.293
2898.	13.770	7.281	5.218	118.9	2.24	0.306
2898.	7.960	0.0	10.041			
3471.	9.000	0.0	10.996			
3871.	9.600	0.0	11.450			
5118.	10.150	0.0	12.426		4.28	
5118.	11.150	0.0	12.578			
6371.	11.190	0.0	12.853			

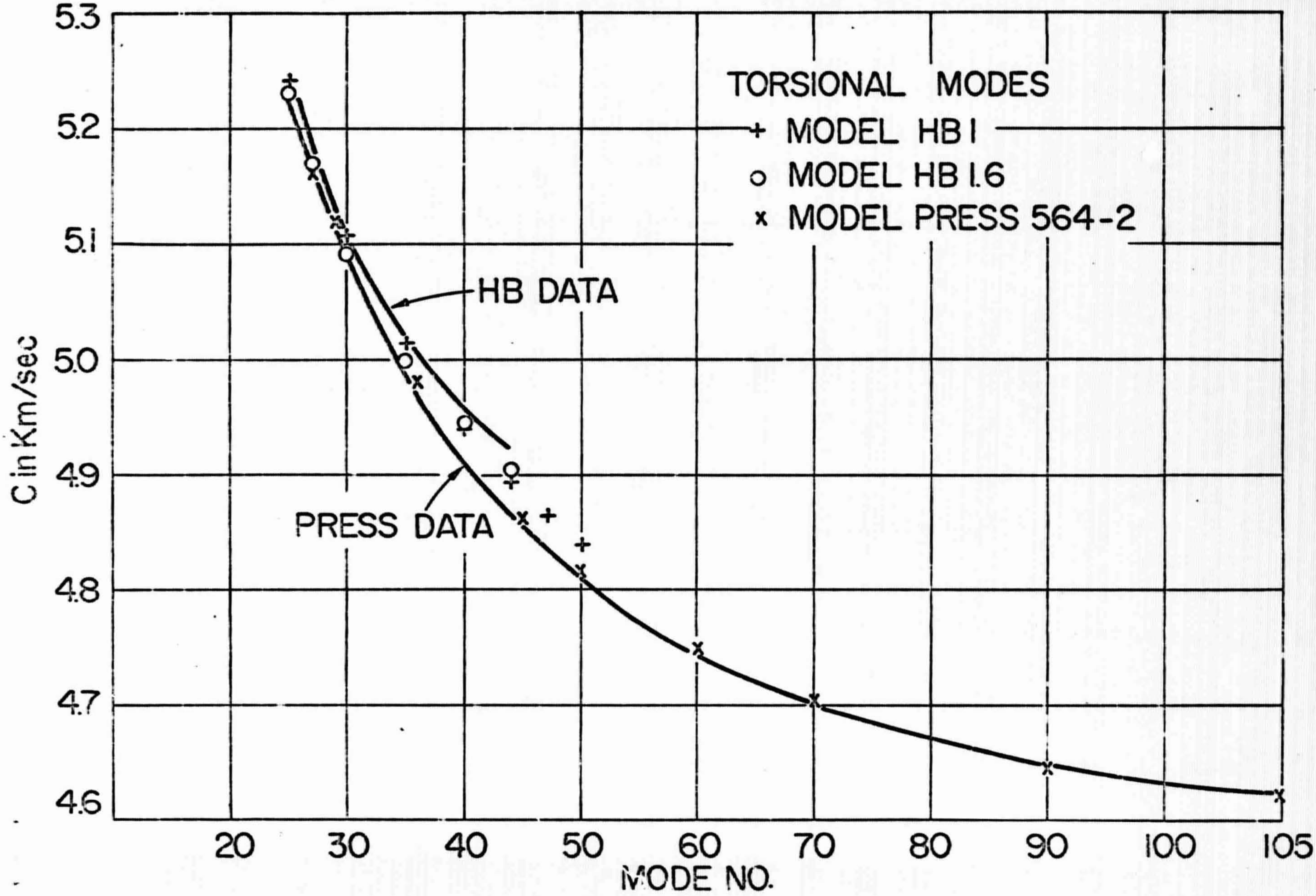

TORSIONAL MODES
+ MODEL HB I
o MODEL HB 1.6
x MODEL PRESS 564-2
HB DATA
PRESS DATA
C in Km/sec
5.3
5.2
5.1
5.0
4.9
4.8
4.7
4.6
20
30
40
50
60
70
80
90
100
105
MODE NO.

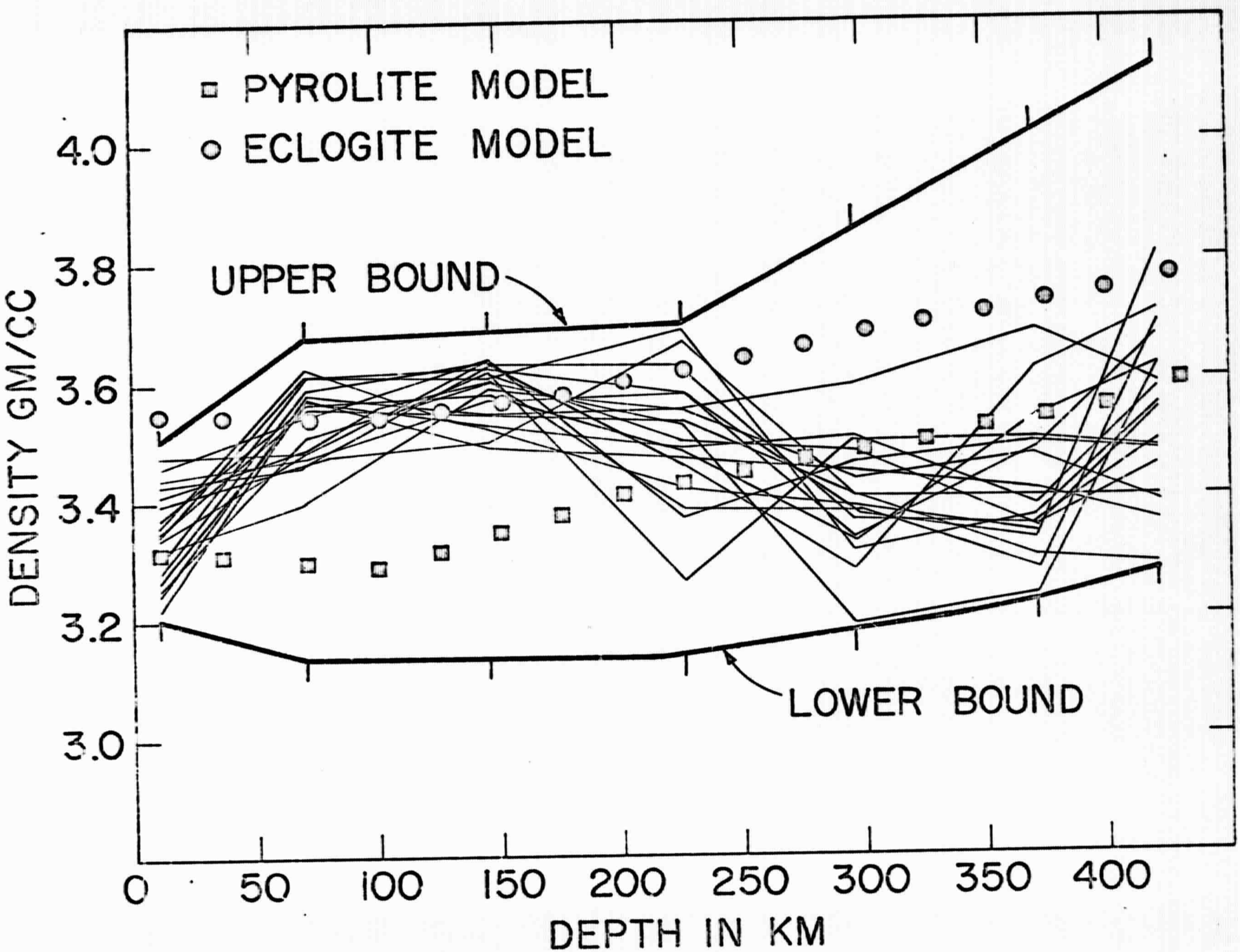

PYROLITE MODEL
ECLOGITE MODEL
UPPER BOUND
LOWER BOUND
DENSITY GM/CC
4.0
3.8
3.6
3.4
3.2
3.0
0
50
100
150
200
250
300
350
400
DEPTH IN KM

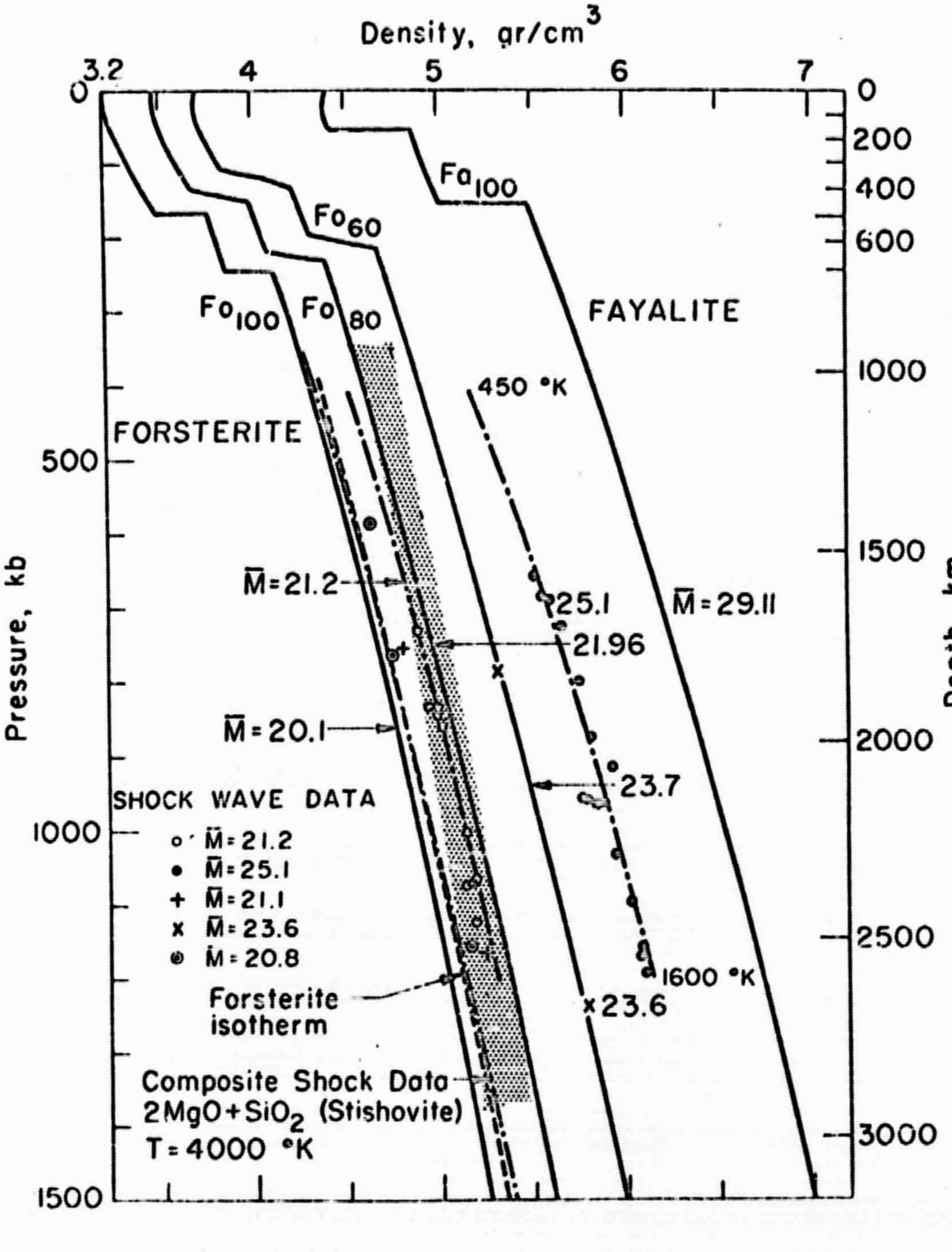

Density, gr/cm3
3.2
4
5
6
7
0
500
1000
1500
Pressure, kb
0
200
400
600
1000
1500
2000
2500
3000
Depth, km
Fa100
Fo60
Fo100
Fo80
FAYALITE
FORSTERITE
450 °K
M̄ = 21.2
25.1
M̄ = 29.11
21.96
M̄ = 20.1
23.7
SHOCK WAVE DATA
M̄ = 21.2
M̄ = 25.1
M̄ = 21.1
M̄ = 23.6
M̄ = 20.8
1600 °K
x 23.6
Forsterite isotherm
Composite Shock Data
2MgO+SiO2 (Stishovite)
T = 4000 °K

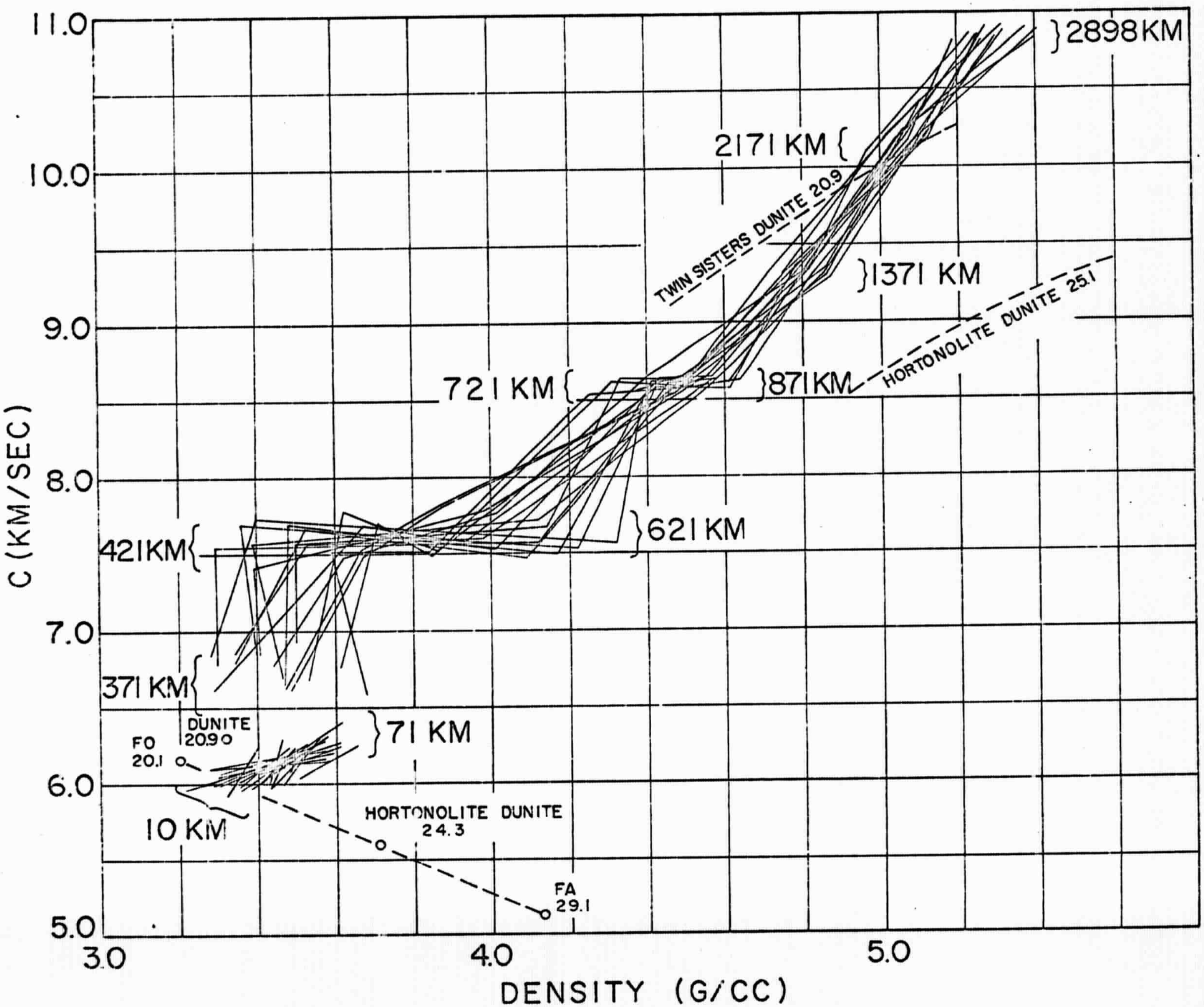

C (KM/SEC)
11.0
10.0
9.0
8.0
7.0
6.0
5.0
3.0
4.0
5.0
DENSITY (G/CC)
2898 KM
2171 KM
TWIN SISTERS DUNITE 20.9
1371 KM
HORTONOLITE DUNITE 25.1
721 KM
871 KM
421 KM
621 KM
371 KM
DUNITE 20.90
FO 20.1
71 KM
10 KM
HORTONOLITE DUNITE 24.3
FA 29.1

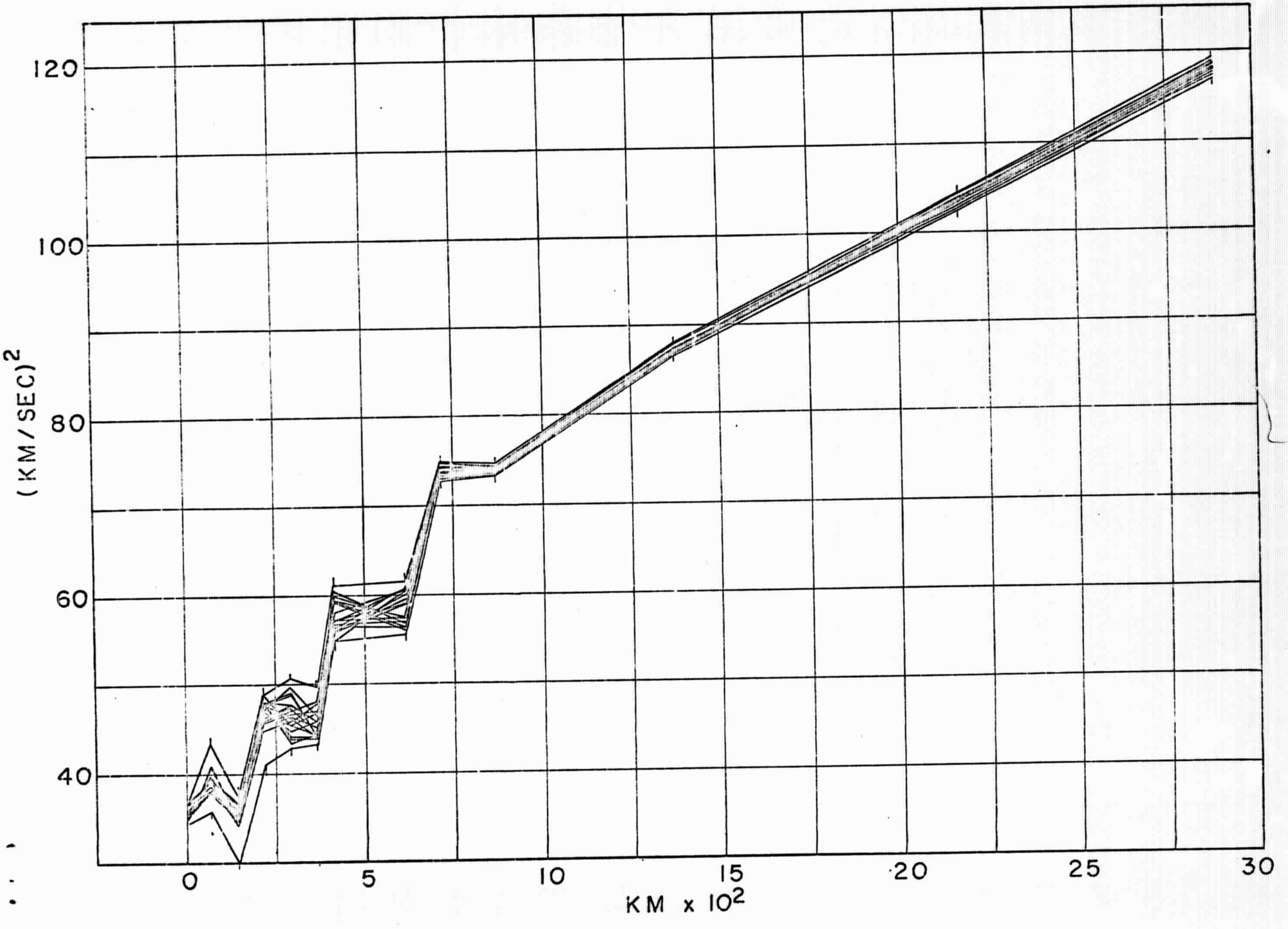

120
100
80
60
40
(KM/SEC)^2
0
5
10
15
20
25
30
KM x 10^2

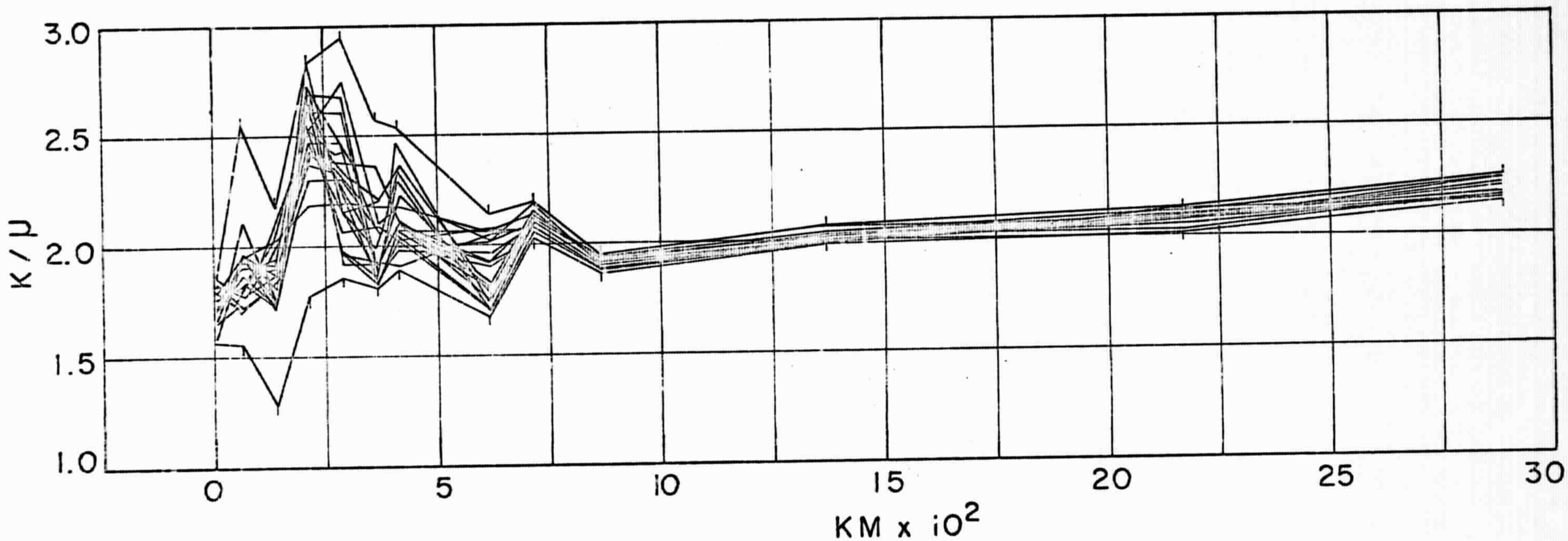

3.0
2.5
2.0
1.5
1.0
K / μ
0
5
10
15
20
25
30
KM x 10²

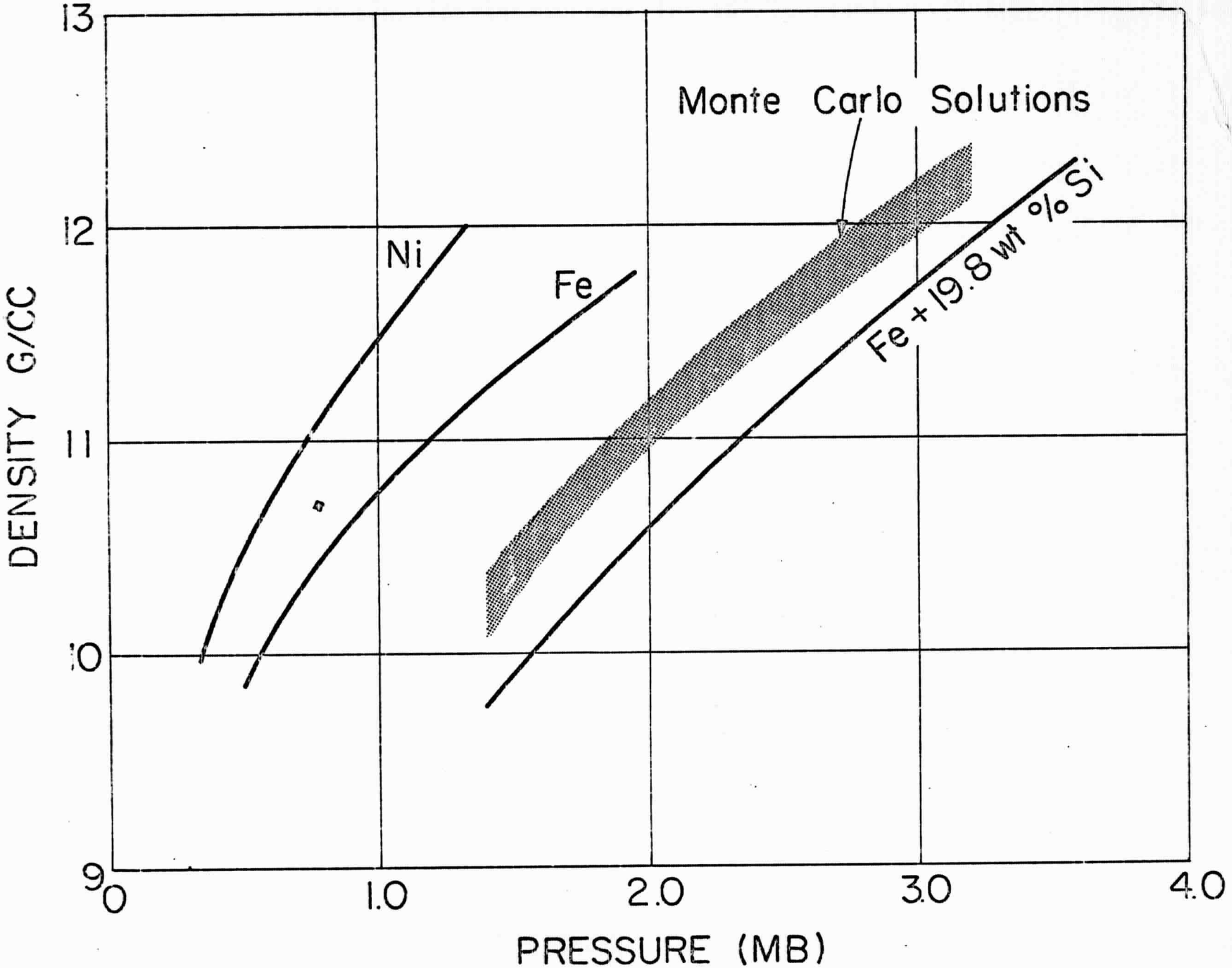

DENSITY G/CC
13
12
11
10
9
0
1.0
2.0
3.0
4.0
PRESSURE (MB)
Ni
Fe
Monte Carlo Solutions
Fe + 19.8 wt % Si